Description of Statistical Models

All models were implemented and compared in R (R Core Development Team, 2021), including random forest regression (Breiman, 2001; Wright & Ziegler, 2017), quantile random forest regression (Meinshausen, 2017), radial support vector machines (Cortes & Vapnik, 1995; Karatzoglou et al., 2004), polynomial support vector machines (Cortes & Vapnik, 1995, Karatzoglou et al., 2004), linear support vector machines (Cortes & Vapnik, 1995; Meyer et al., 2021), ridge regression (Hoerl & Kennard, 1970; Zou & Hastie, 2020), and lasso regression (Tibshirani, 1996; Zou & Hastie, 2020).

Random forest models build multiple decision trees and bootstrap training samples within each tree. A random sample of *m* predictors is chosen as a split candidate at each split in each decision tree. This injection of randomness usually improves predictive performance as it reduces overfitting. Quantile random forests are similar but have the additional benefit of providing prediction intervals by estimating conditional quantiles. When used for regression, the objective function for support vector machines it to minimize the l2-norm of the coefficient vector. The error term is then handled in the constraints of the minimization function where the absolute error is set to be less than or equal to a specified margin, and this specified margin is the error, or ϵ (epsilon). Epsilon (the width of the margin) can then be tuned to an optimal accuracy. Radial and polynomial support vector machines use the same underlying theory but enlarge the feature space using quadratic, cubic or higher order polynomial functions of the predictors to achieve non-linearity. Ridge regression is very similar to least squares with the exception that a penalty term λ is introduced. λ is multiplied by the sum of the squared regression coefficients and then added to the residual sum of square error. This is called a shrinkage penalty (or L2 regularization) and has the effect of shrinking the coefficients towards 0 (but not to 0) at larger λ values. This penalty is useful for dealing with multicollinearity. Lasso regression also implements a shrinkage penalty but is instead called L1 regularization and λ is multiplied by the absolute values of the regression coefficients, and this can force the coefficients to 0.

Supplemental Figures

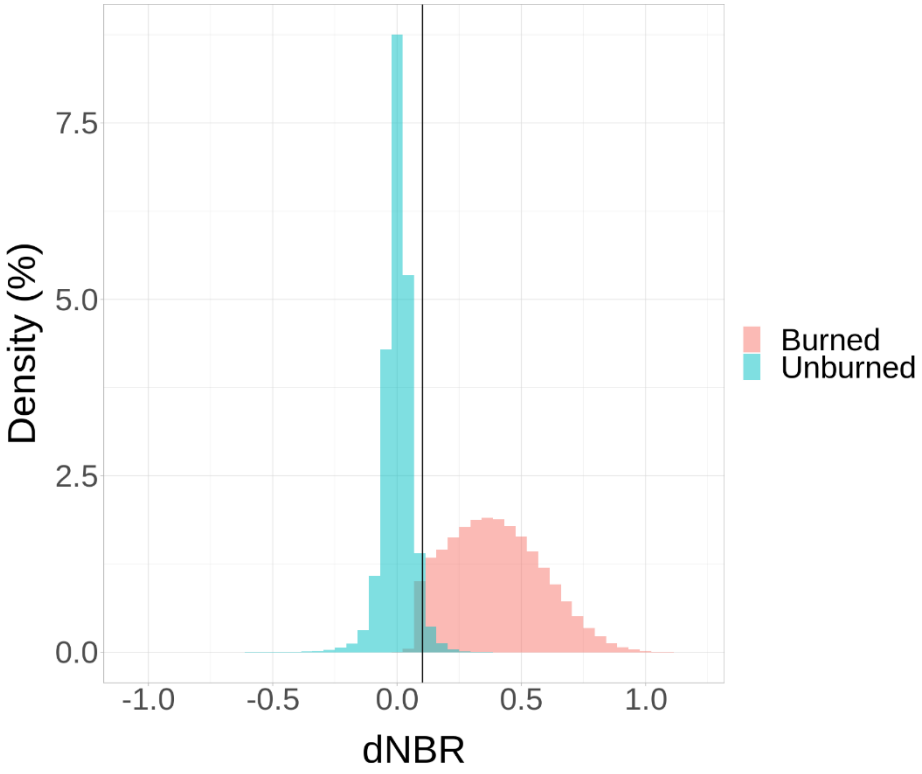

Figure S1. Differenced Normalized Burn Ratio (dNBR) threshold for determining burn status of 30 m pixels in Landsat imagery. The distributions show dNBR for burned and unburned control field sites contained in the Walker et al. (2020a) combustion database (including our artificial inflation of control sites by using dNBR in years prior to the fire event). A dNBR threshold of 0.084 (vertical black line) minimized commission and omission errors at the site-level.

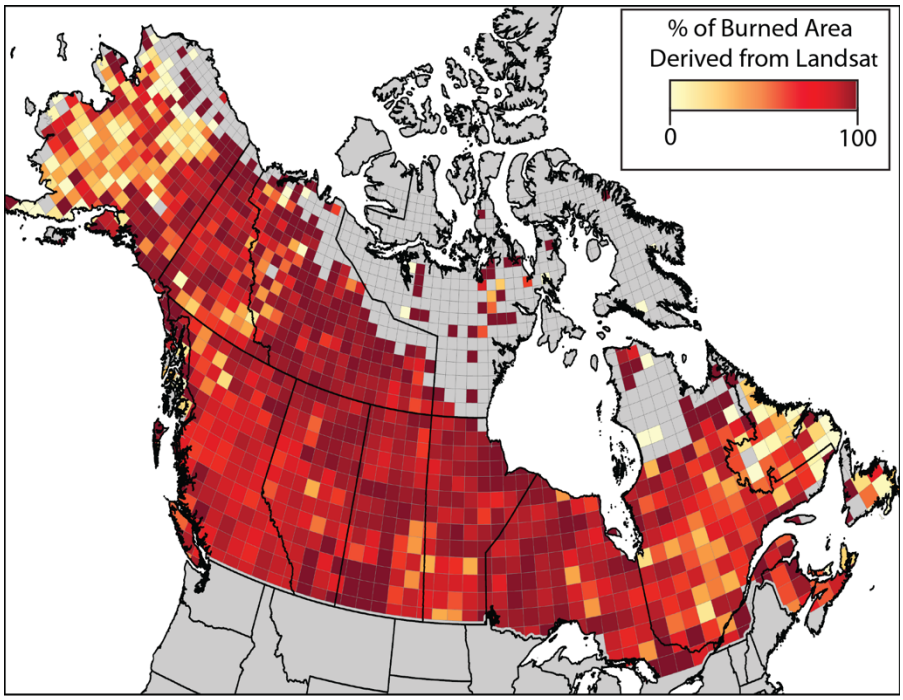

Figure S2. Percent of the total ABoVE-FED burned area product derived from Landsat (quality flag bands 0-1), aggregated to a 70 km grid.

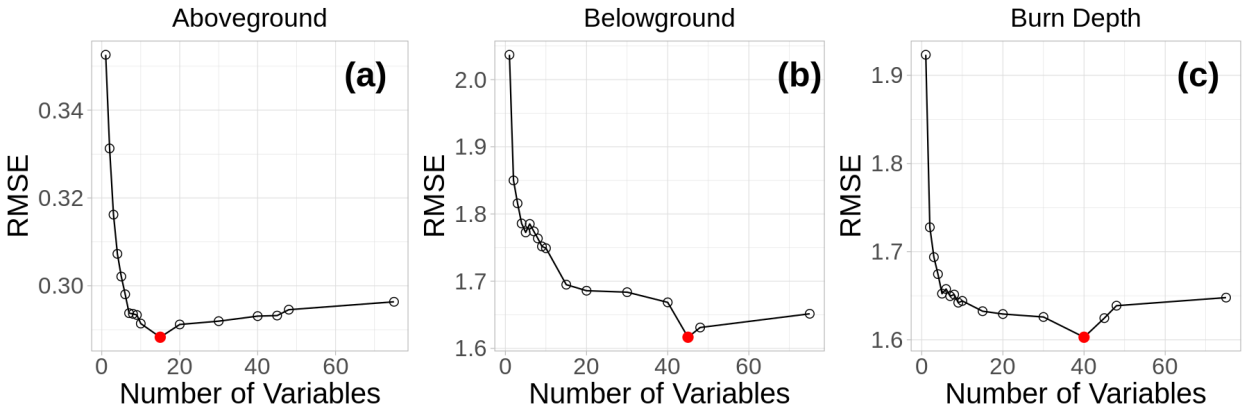

Figure S3. Recursive Feature Elimination implementation to find the optimal number of predictor variables for the aboveground (a), belowground (b) and burn depth (c) models. The red dot in each plot represents the point at which Root Mean Square Error (RMSE) was minimized. Associated variables were then used in final model implementations.

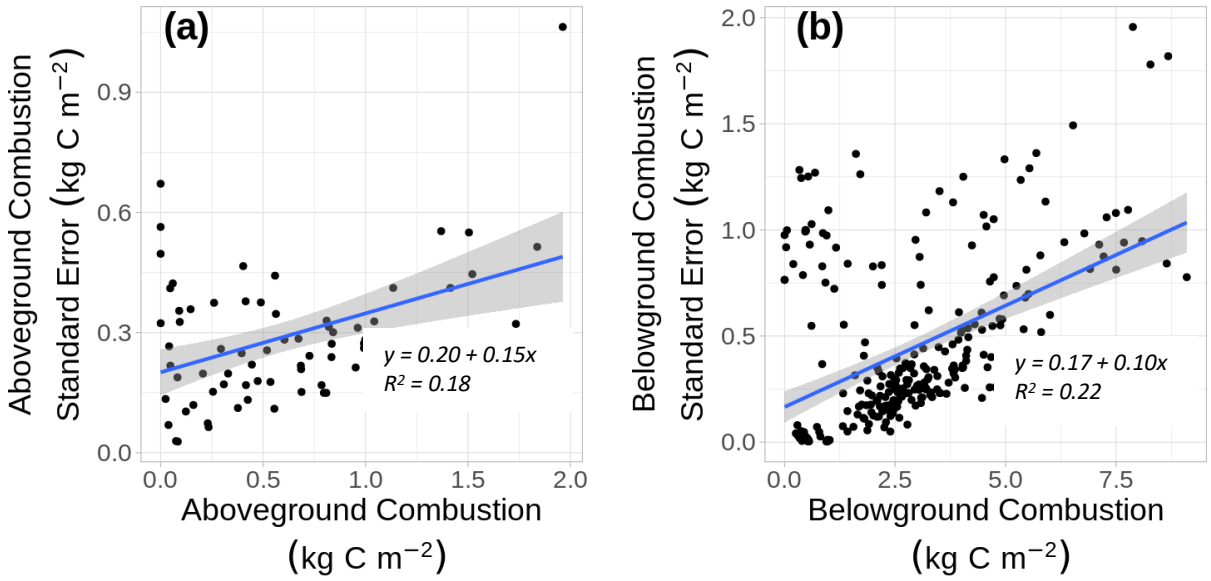

Figure S4. Linear regression models used to estimate the standard error of combustion for aboveground (a) and belowground (b) field samples for which standard error was not directly measured. Regression equations and R^2 from the model fits are shown.

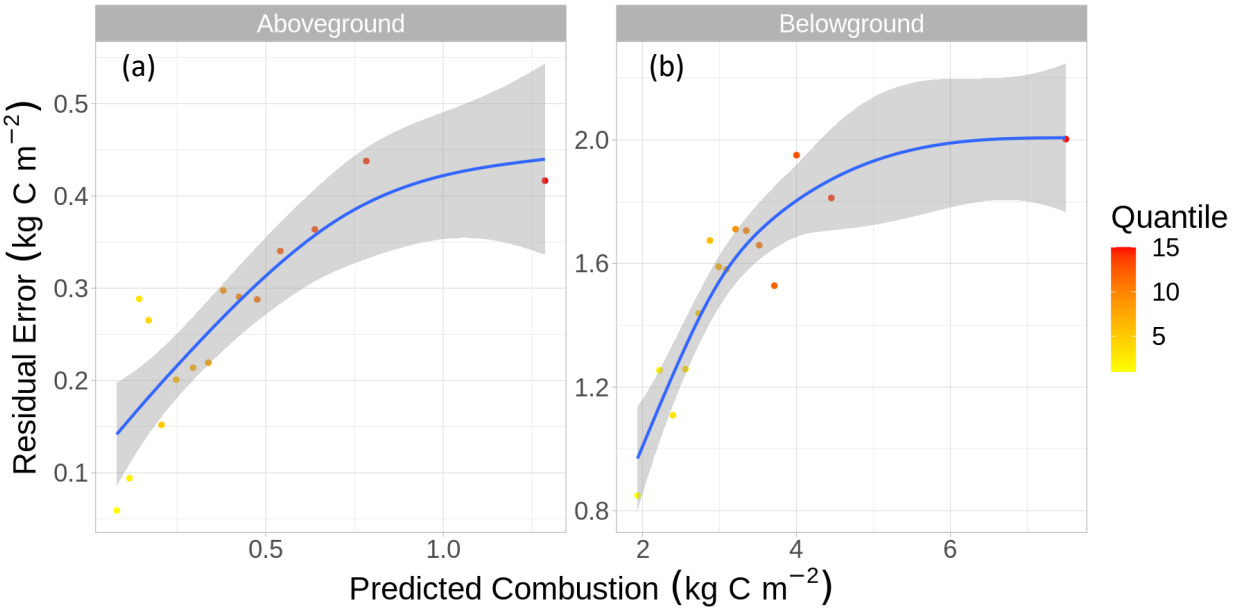

Figure S5. General Additive Models used to estimate residual errors as a function of predicted combustion. Points represent the relationships across 15 quantiles for the primary aboveground (a) and belowground (b) combustion random forest models.

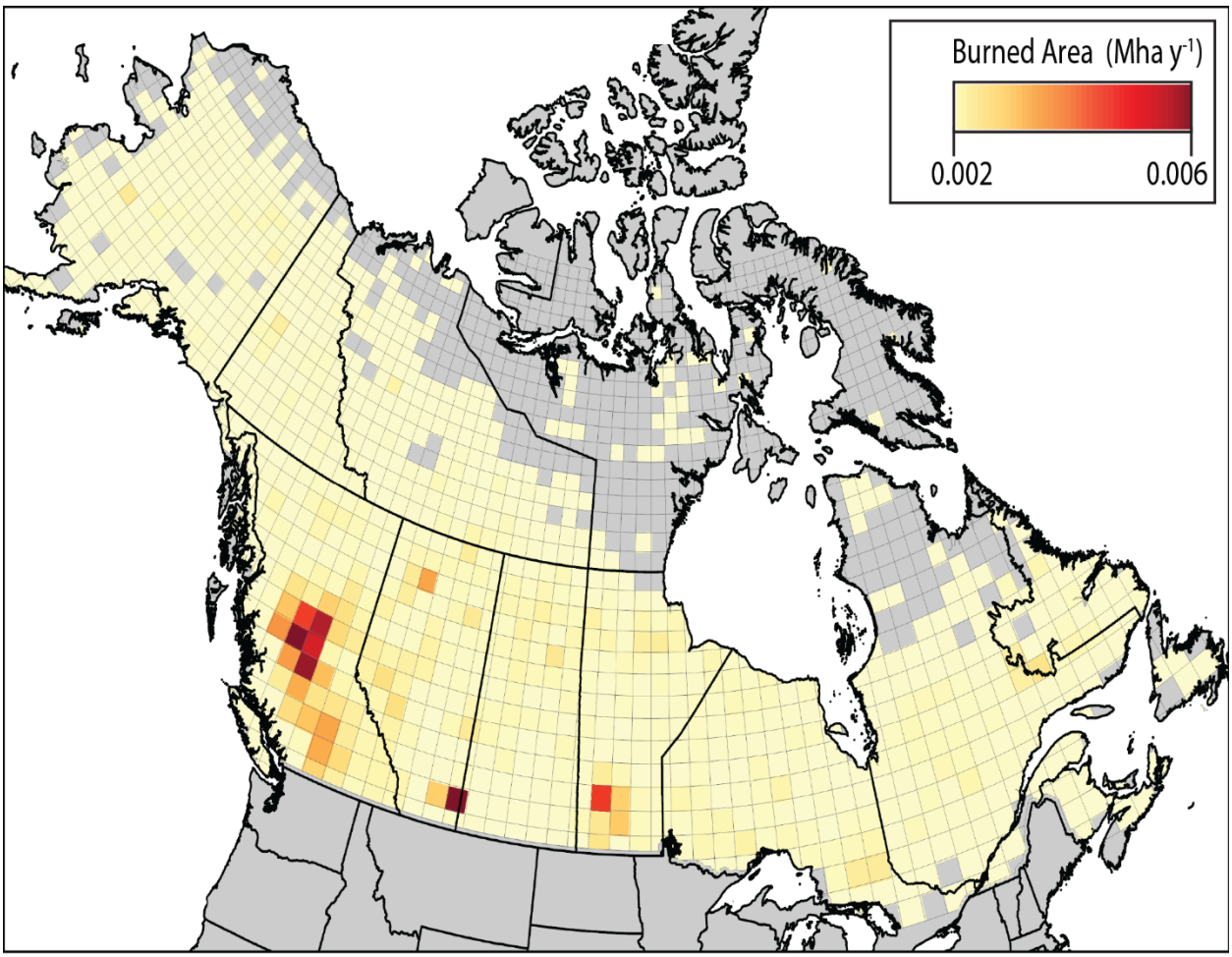

Figure S6. Burned area from ABoVE-FED located outside of the NLFD fire polygons, aggregated to a 70 km grid. Burned area outside the NLFDB polygons constituted 7% of the total domain-wide burned area.

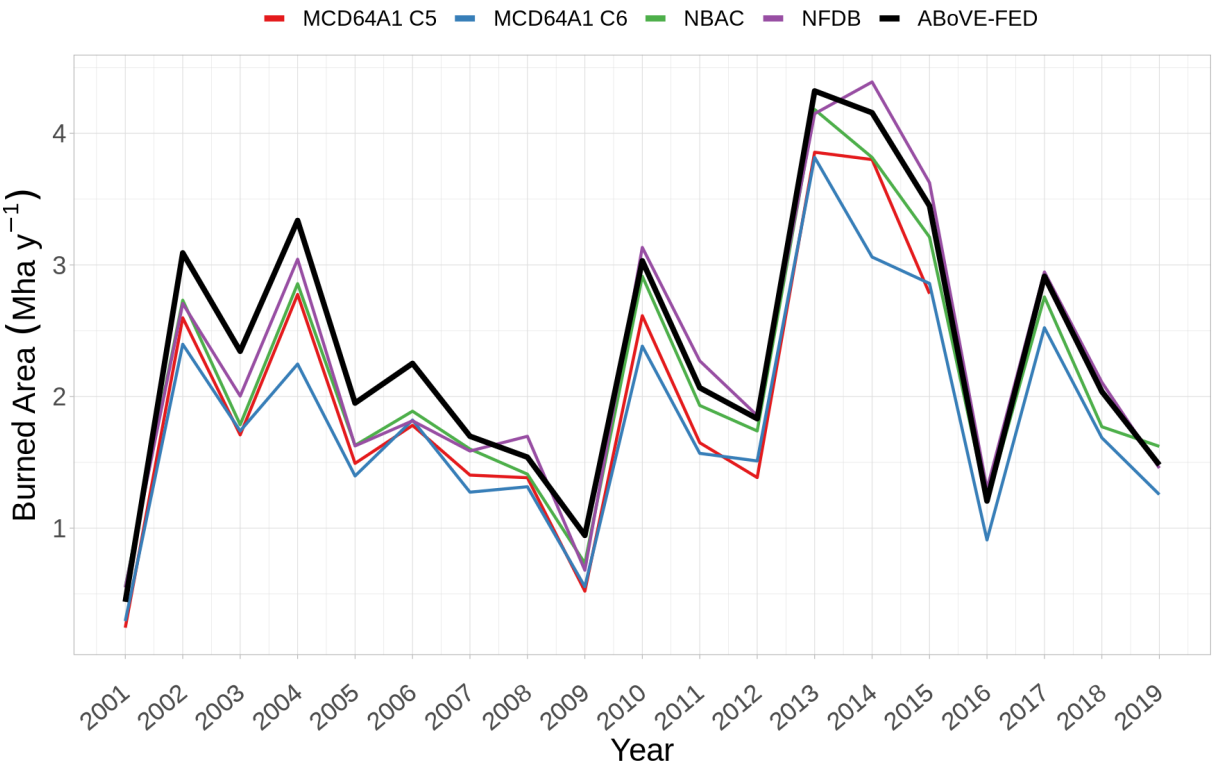

Figure S7. Comparison of ABoVE-FED burned area across Canada to MODIS MCD64A1 Collection 5 (C5), Collection 6 (C6), the Canadian National Burned Area Composite (NBAC), and the Alaskan and Canadian National Fire Databases (NFDB).

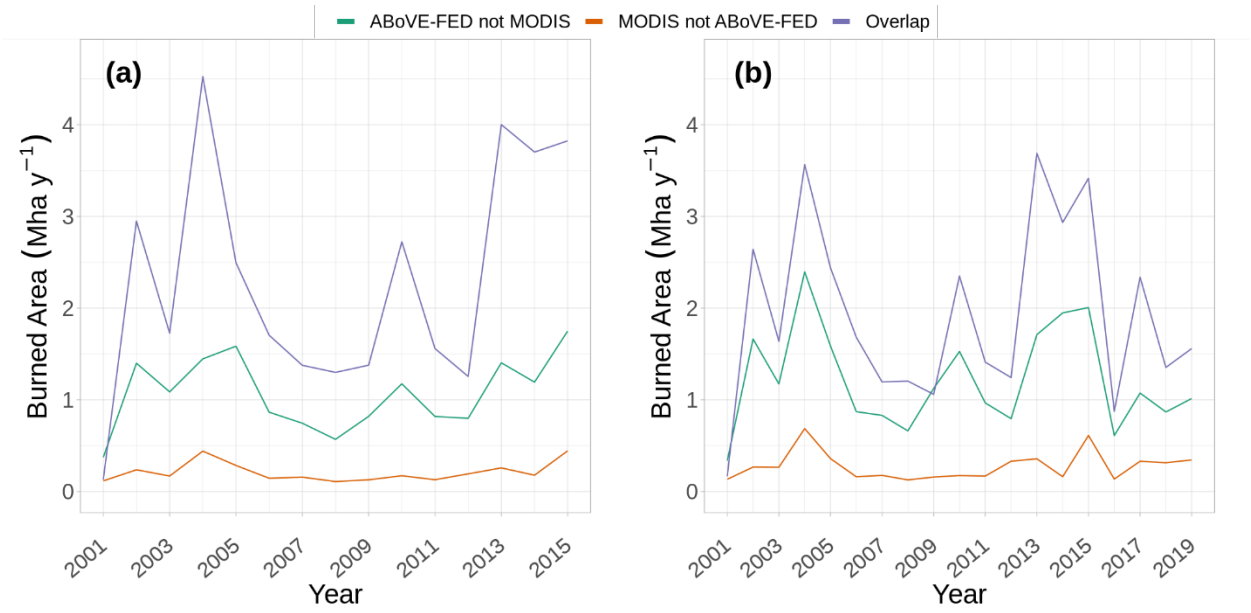

Figure S8. Comparison of ABoVE-FED burned area to the MODIS Collection 5 (a) and Collection 6 (b) burned area products across Alaska and Canada. Lines are shown for pixels where MODIS detects fires but ABoVE-FED does not (MODIS not ABoVE-FED), where ABoVE-FED detects burned area but MODIS does not (ABoVE-FED not MODIS), and where both products detect burned area (Overlap).

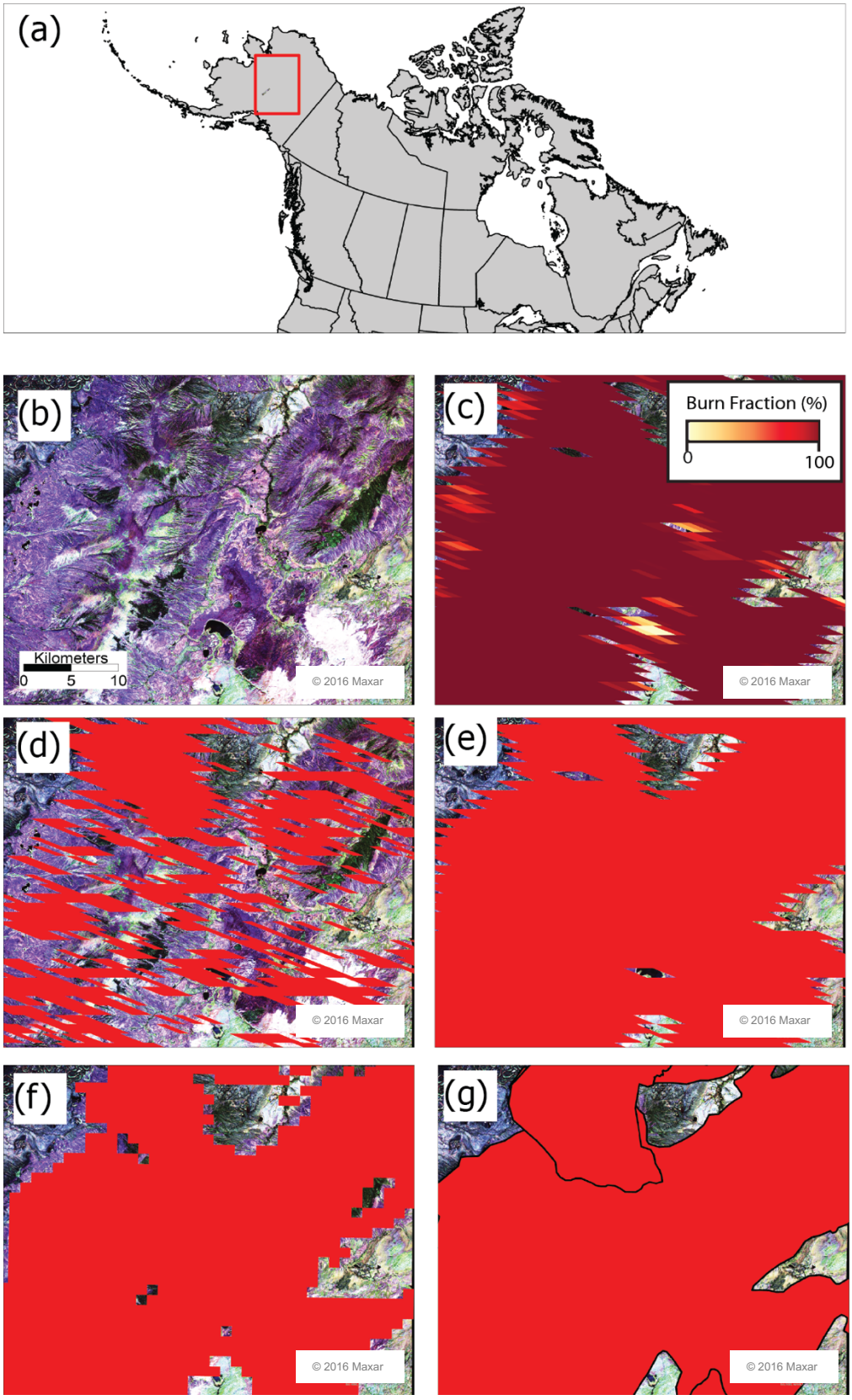

Figure S9. Comparison of high-resolution imagery and burned products for a fire in Alaska in 2016 (a). Panels show Worldview-2 imagery ©2016 DigitalGlobe, Inc., a Maxar company, NextView License (b, fire shown in pink and purple shades): ABoVE-FED (c), MODIS Collection 6 (d), MODIS Collection 5 (e), AKFED (f), and the ALFD (g).

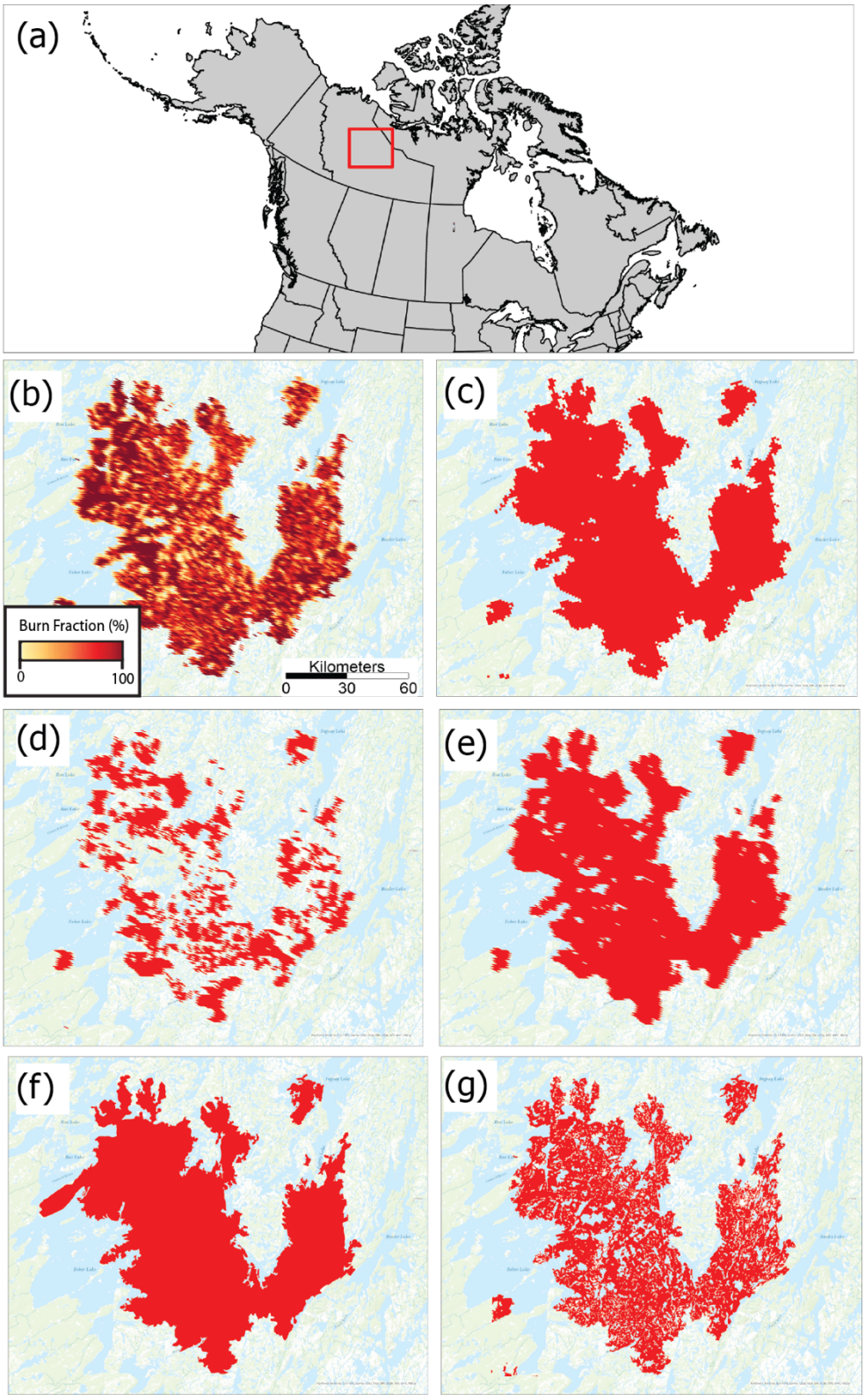

Figure S10. Comparison of a 2014 fire event in the Northwestern territories (a) for ABoVE-FED (b), AKFED (c), MCD64A1 Collection 6 (d), MCD64A1 Collection 5 (e), the Canadian National Fire Database (f) and the National Burn Area Composite (g). Basemap Sources: Esri, HERE, Garmin, USGS, NGA, EPA, USDA, NPS, AAFC and NRCran.

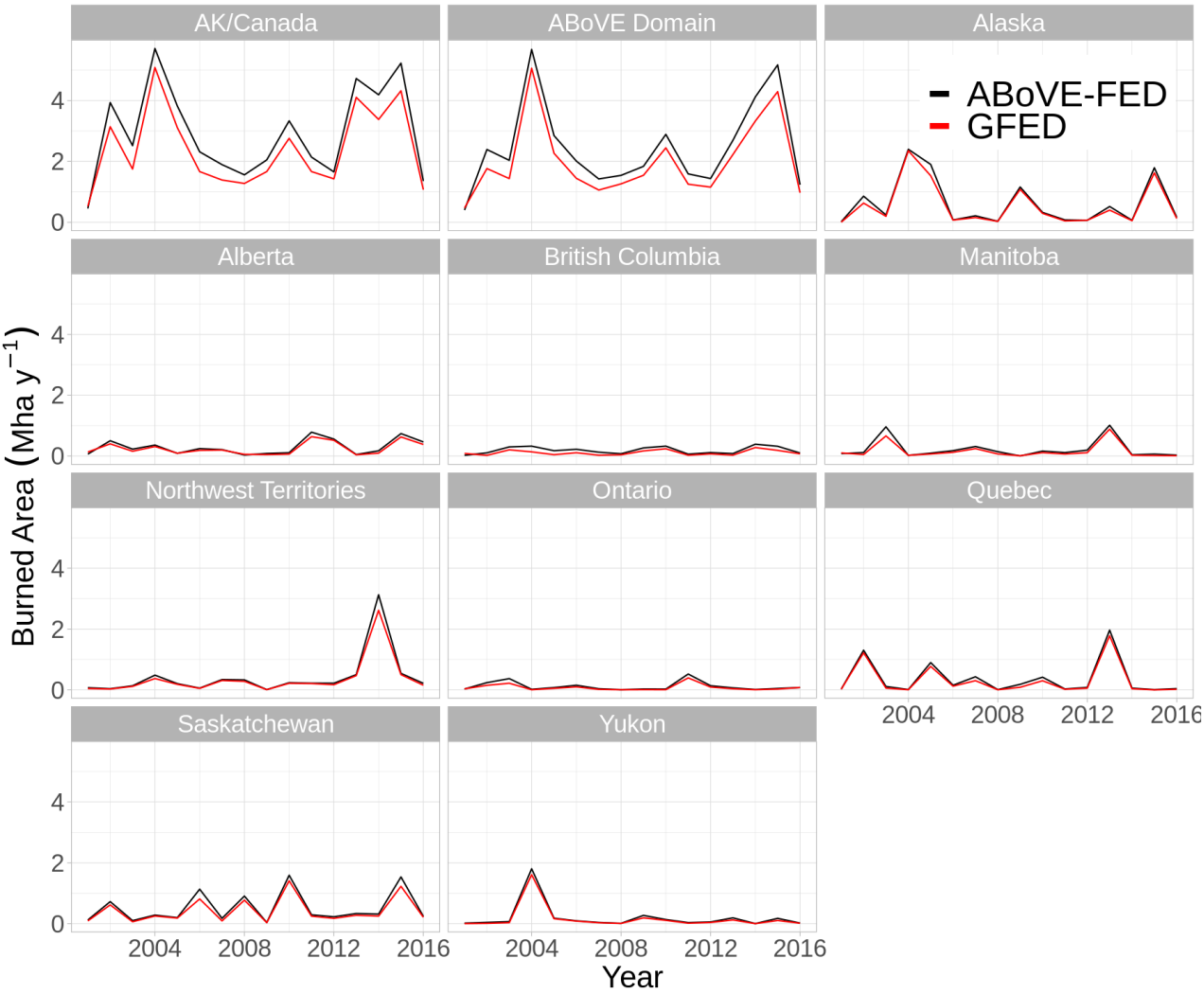

Figure S11. Burned area across all of Alaska and Canada, the ABoVE Domain and individual Alaska and Canadian provinces and Territories during 2001-2016 for GFED4s and ABoVE-FED.

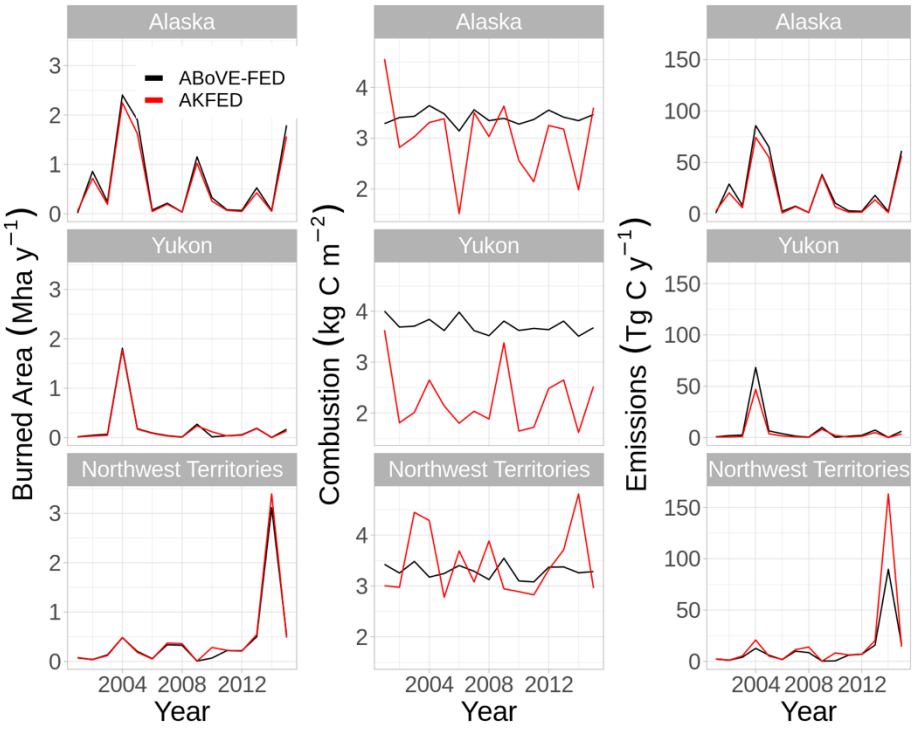

Figure S12. Burned area, total carbon emissions, and mean annual combustion for ABoVE-FED and AKFED in Alaska, the Yukon Territory, and the Northwest Territories between 2001 - 2015.

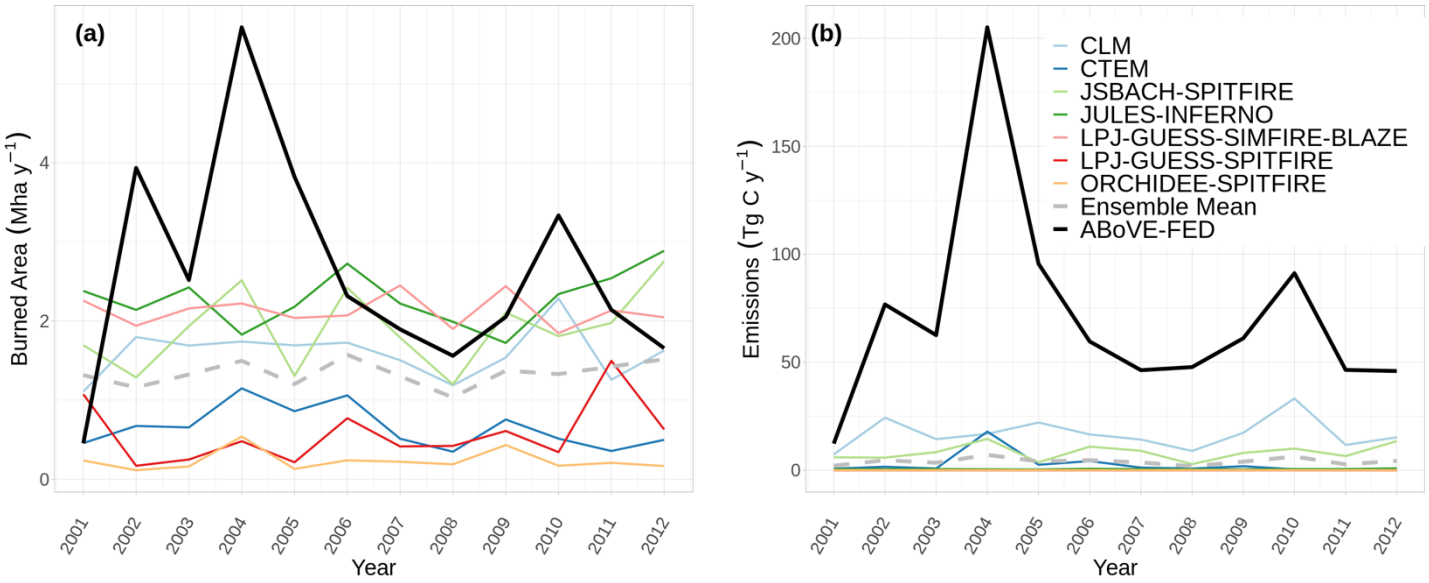

Figure S13. Comparison of burned area (a) and emissions (b) between ABoVE-FED and FireMIP. Individual model runs as well as the ensemble mean are shown for FireMIP. Panel (a) shows burned area across Alaska and Canada and panel (b) shows carbon emissions for the ABoVE domain.

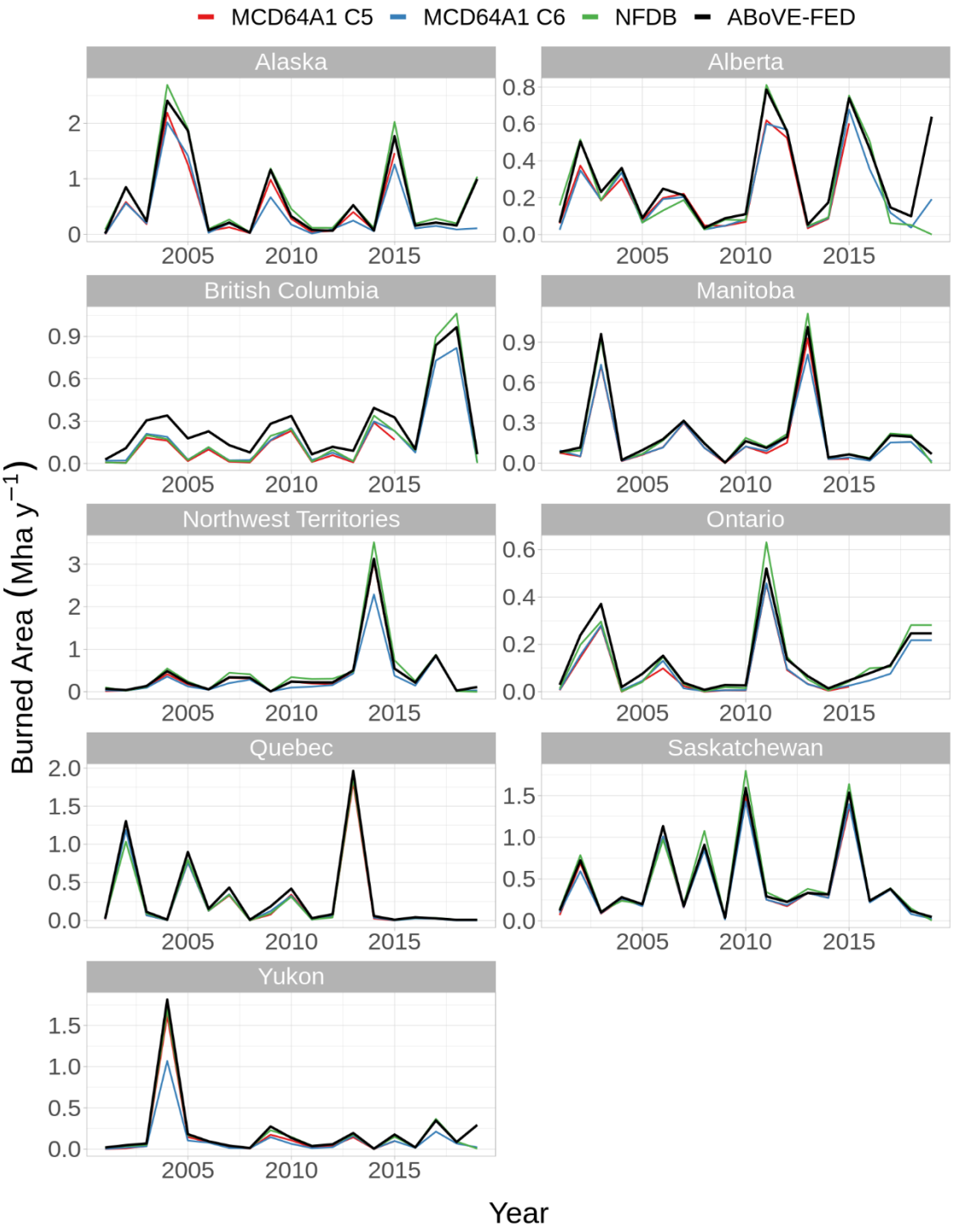

Figure S14. Burned area across Alaska and Canadian provinces and territories during 2001-2019 for MODIS MCD64A1 Collection 5 (C5), Collection 6 (C6), the NFDB, NBAC, and ABoVE-FED.

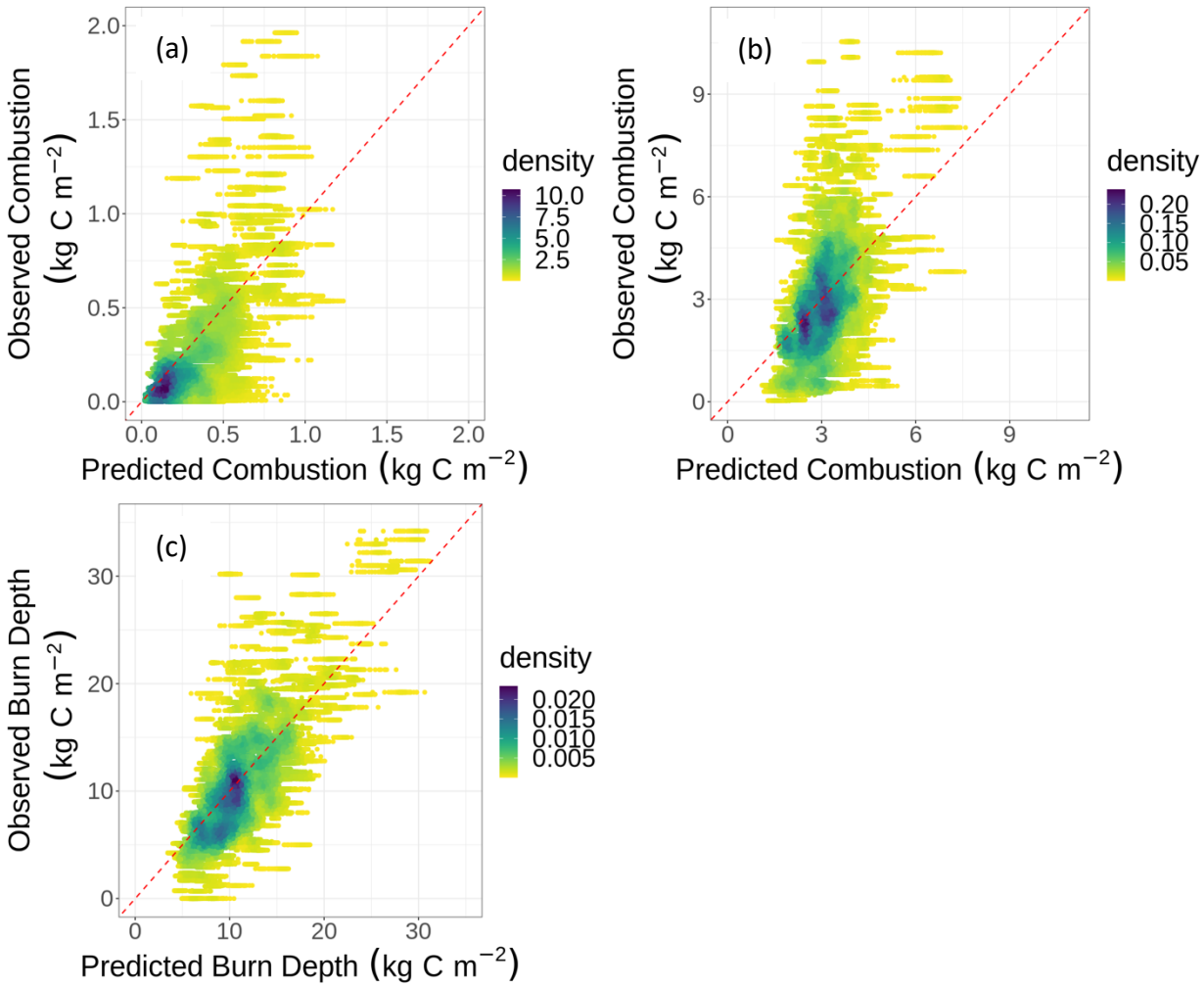

Figure S15. Comparison of observed and predicted combustion across a 10-fold cross-validation repeated 100 times for the aboveground combustion, (a) belowground combustion (b), and burn depth (c) models.

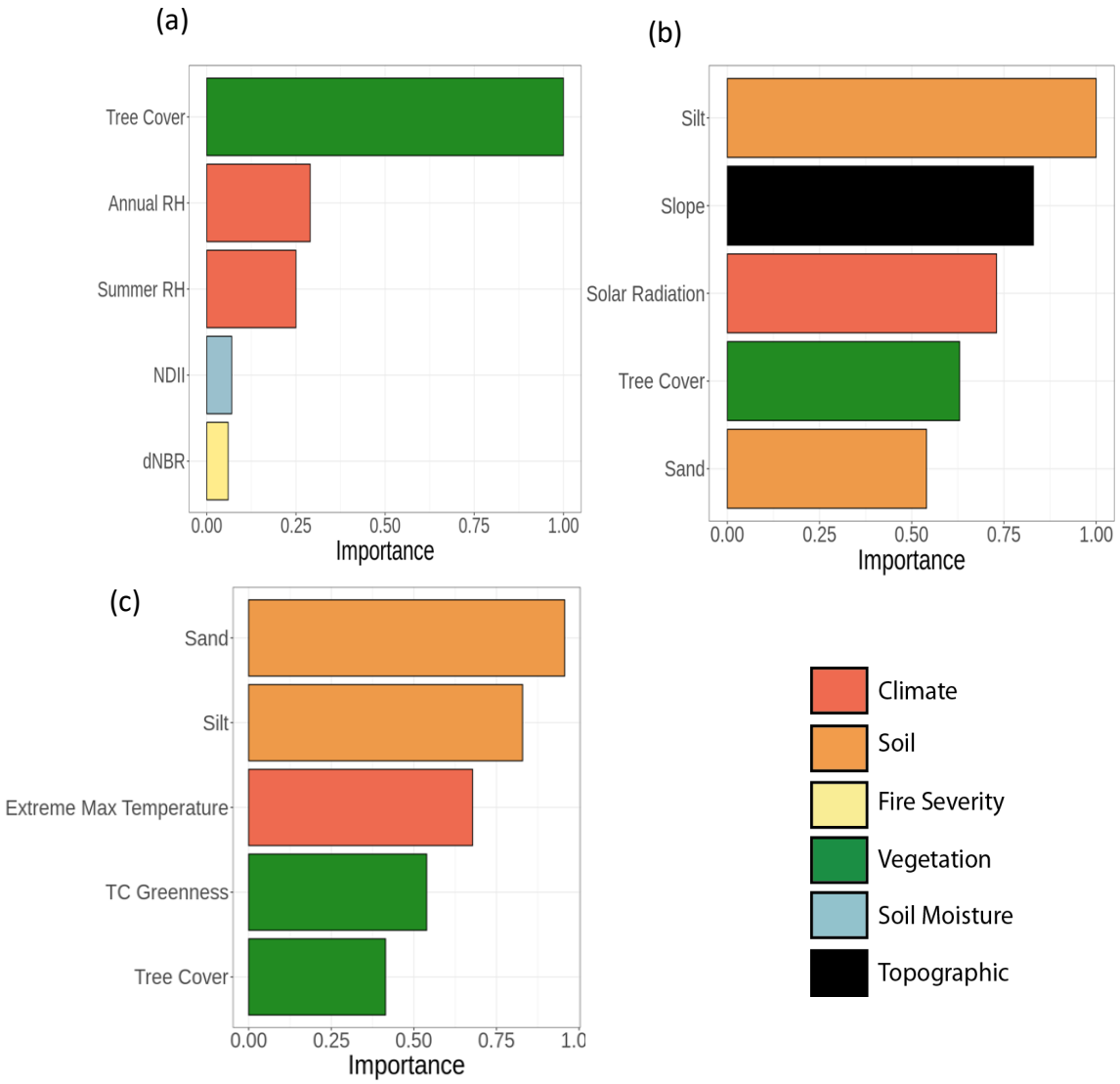

Figure S16. Feature importance for the primary aboveground combustion (a), belowground combustion (b), and burn depth (c) models. Variable names and meanings are described in Table S1, including Tree Cover, Annual Relative Humidity (Annual RH), Summer Relative Humidity (Summer RH), Normalized Difference Infrared Index (NDII), and the differenced Normalized Burn Ratio (dNBR), Silt % at 30 cm (Silt), Slope, Solar Radiation Tree Cover (%) Sand % at 30c m (Sand), Extreme Maximum Temperature, and Tasseled Cap Greenness (TC Greenness). Variables are color coded by category.

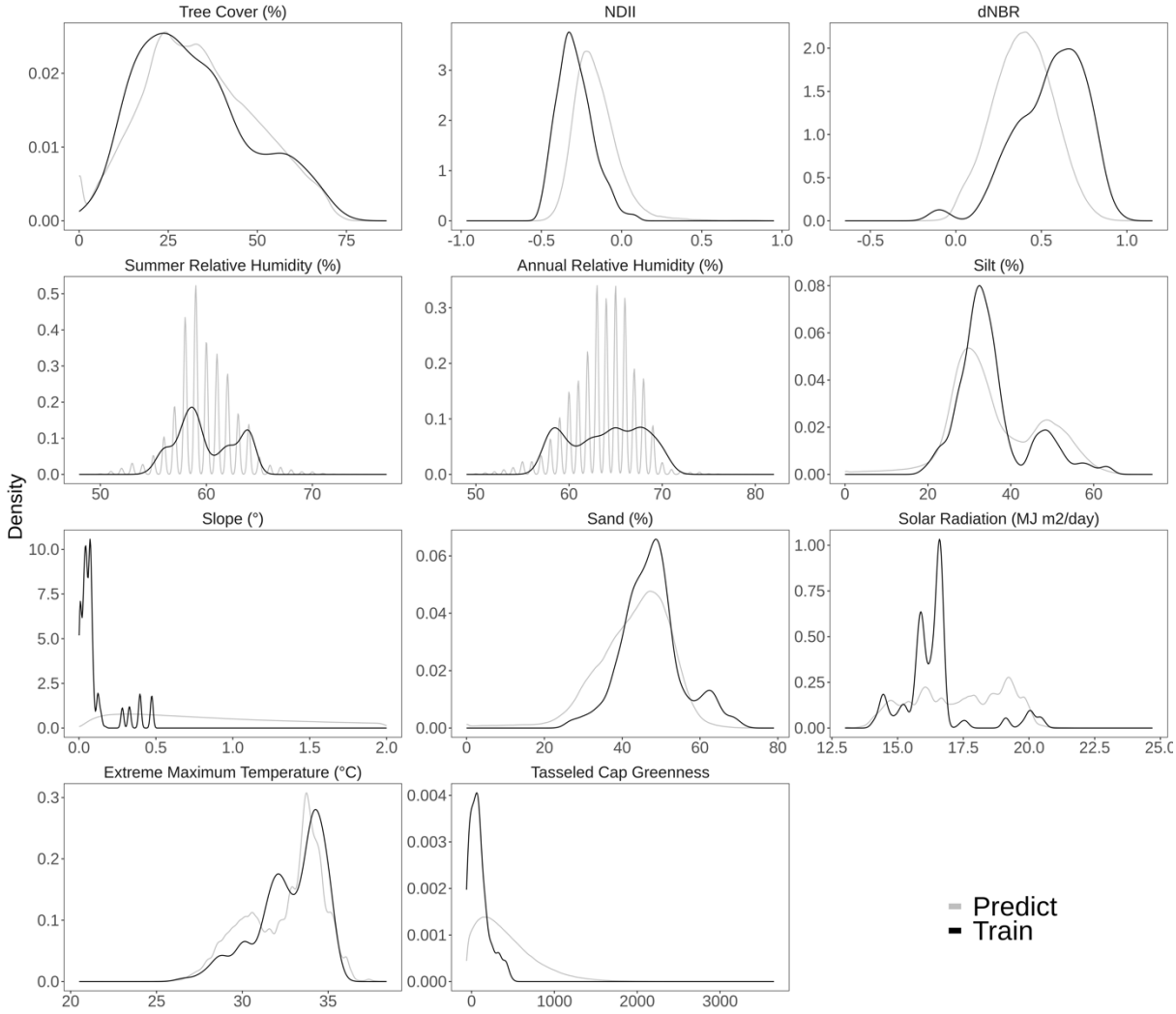

Figure S17. Frequency distributions for the most influential predictor variables (Figure S9) between the training set of field observations and predicting set across the entire domain. Note that the x-axis for slope has been limited to 2 degrees for visual purposes; predictions above 2 degrees occur, but in low frequency.

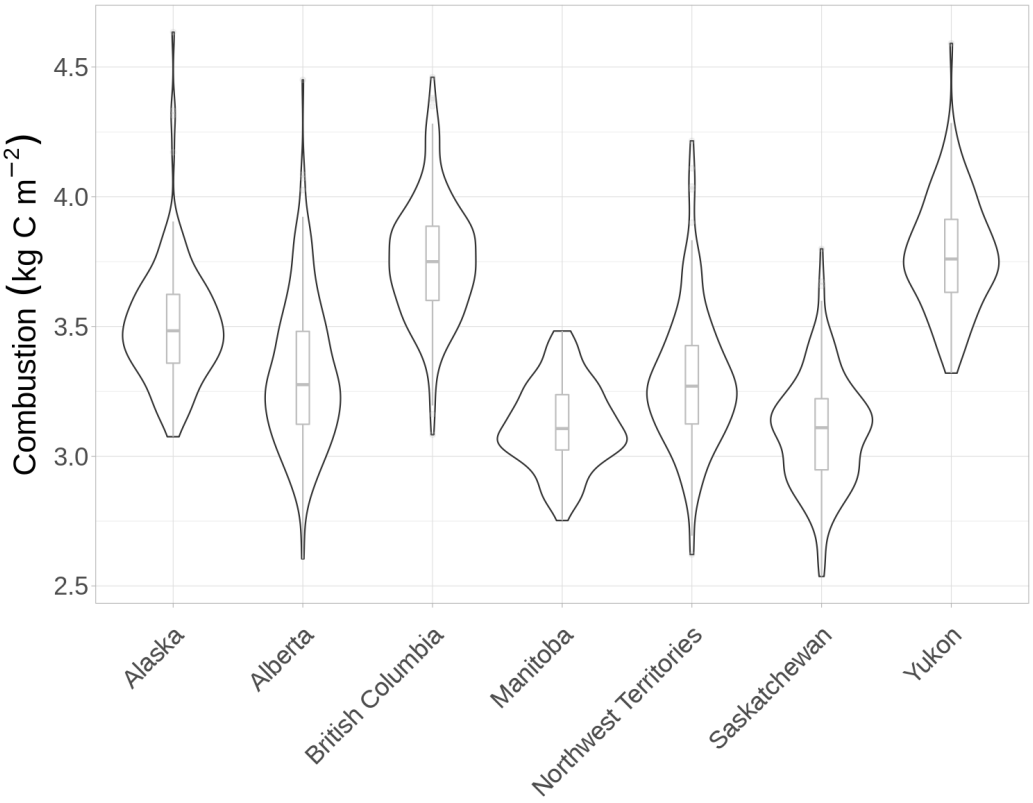

Figure S18. Violin plots of variation in combustion estimates between 2001-2019 for each state and Canadian provinces and territories.

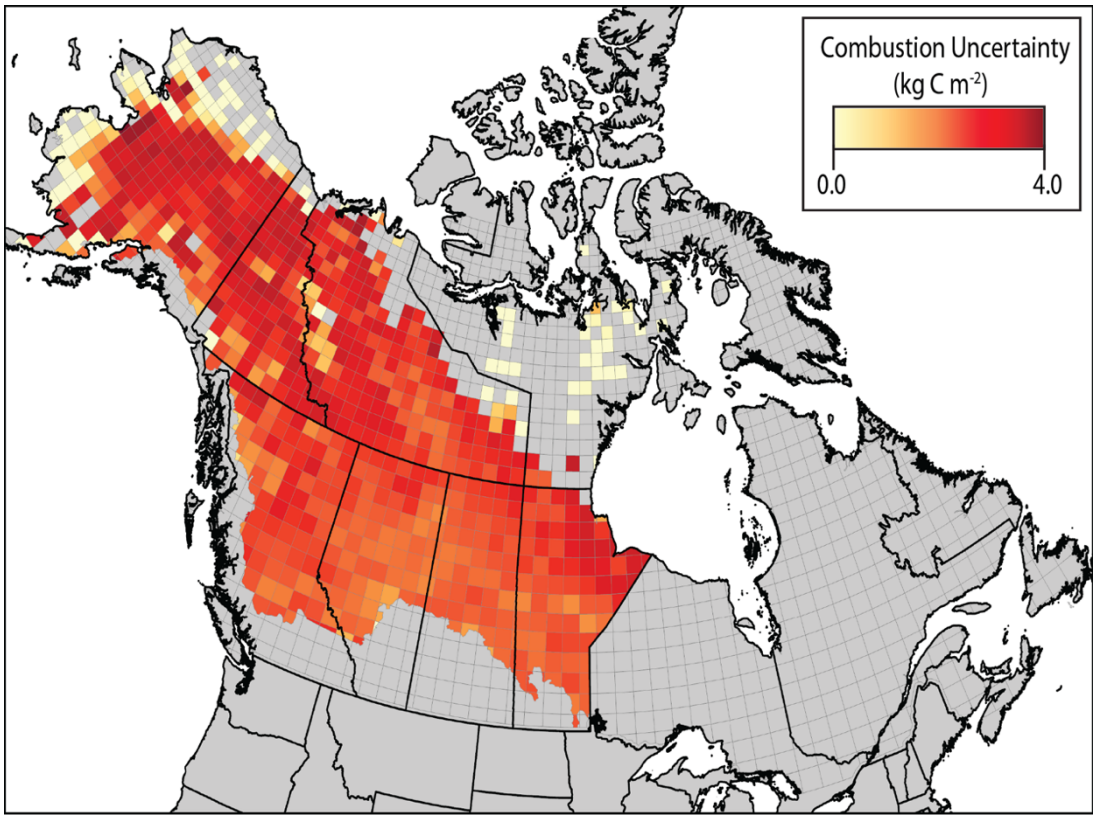

Figure S19. Mean uncertainty in pixel-level combustion derived from the Monte Carlo analysis, aggregated to a 70 km grid.

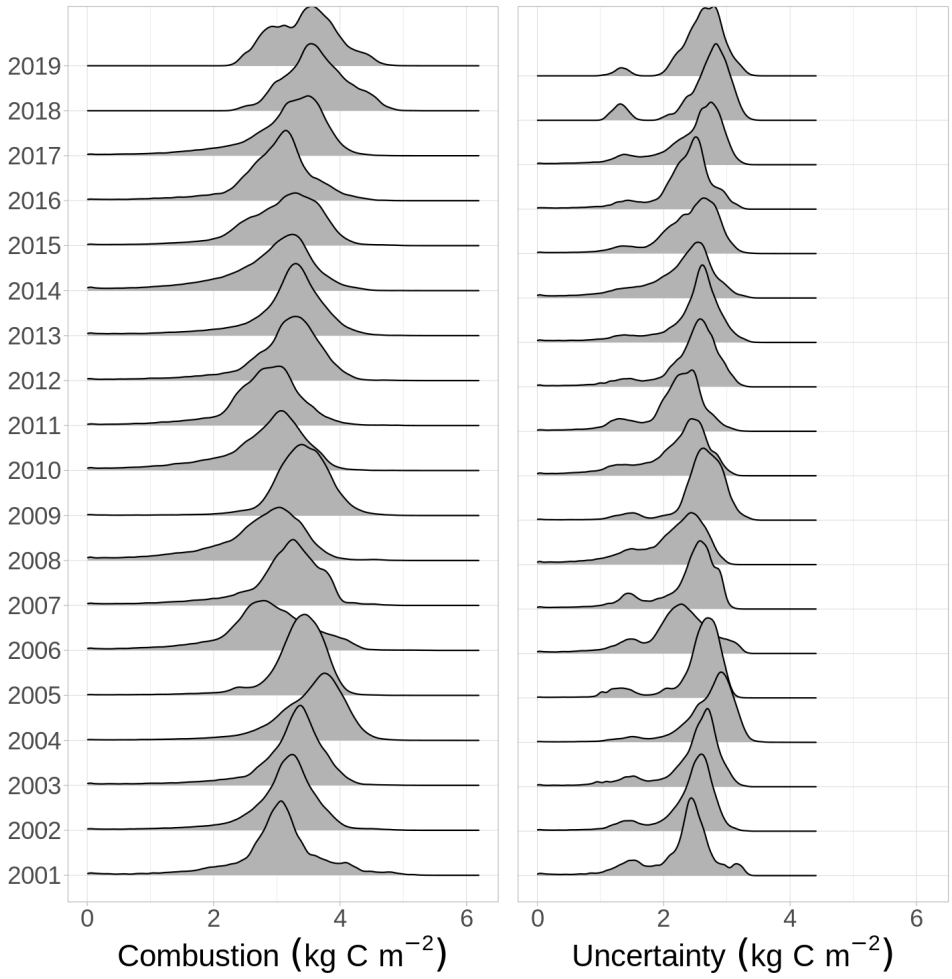

Figure S20. Distributions of predicted combustion and pixel-level uncertainty based on the Monte Carlo analysis for each year in the ABoVE extended domain.

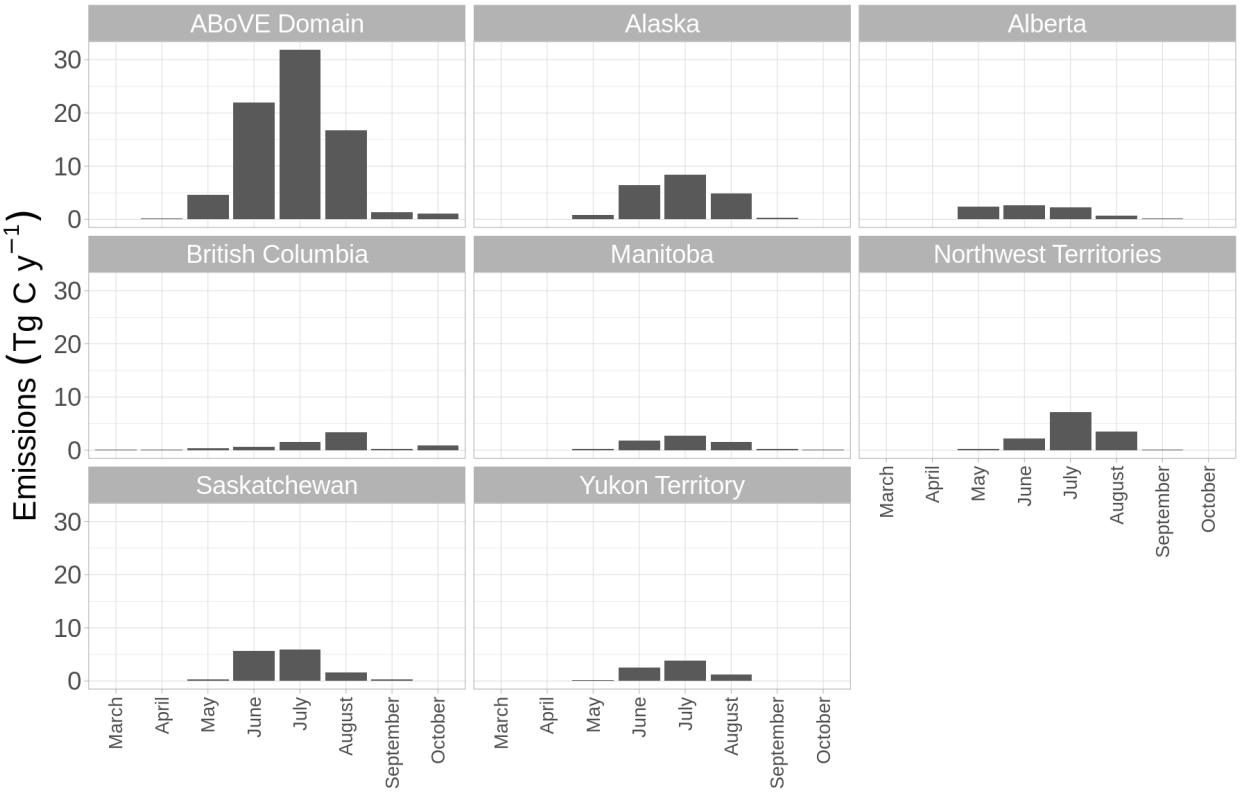

Figure S21. Variation in mean monthly carbon emissions by state / province / territory. December-February are not shown due to small frequency of fire.

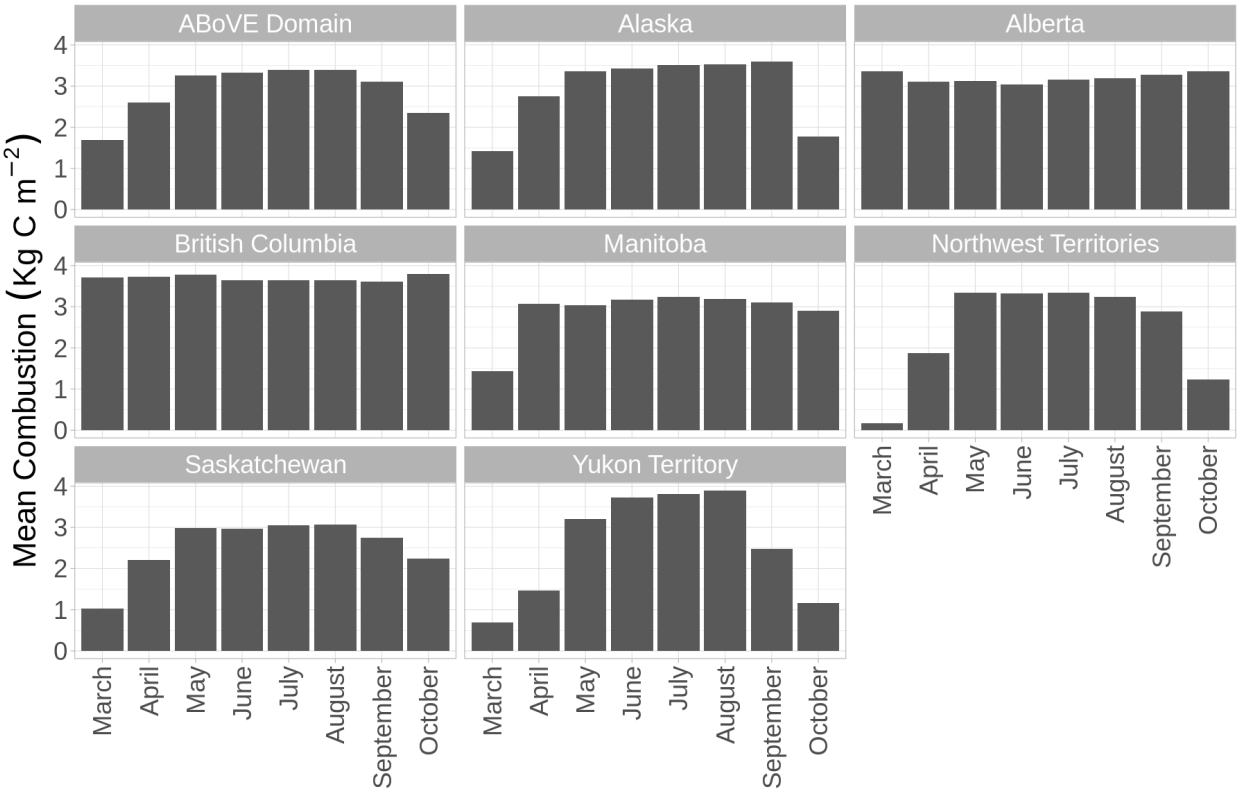

Figure S22. Variation in mean monthly combustion by state / province / territory. December-February are not shown due to small frequency of fire.

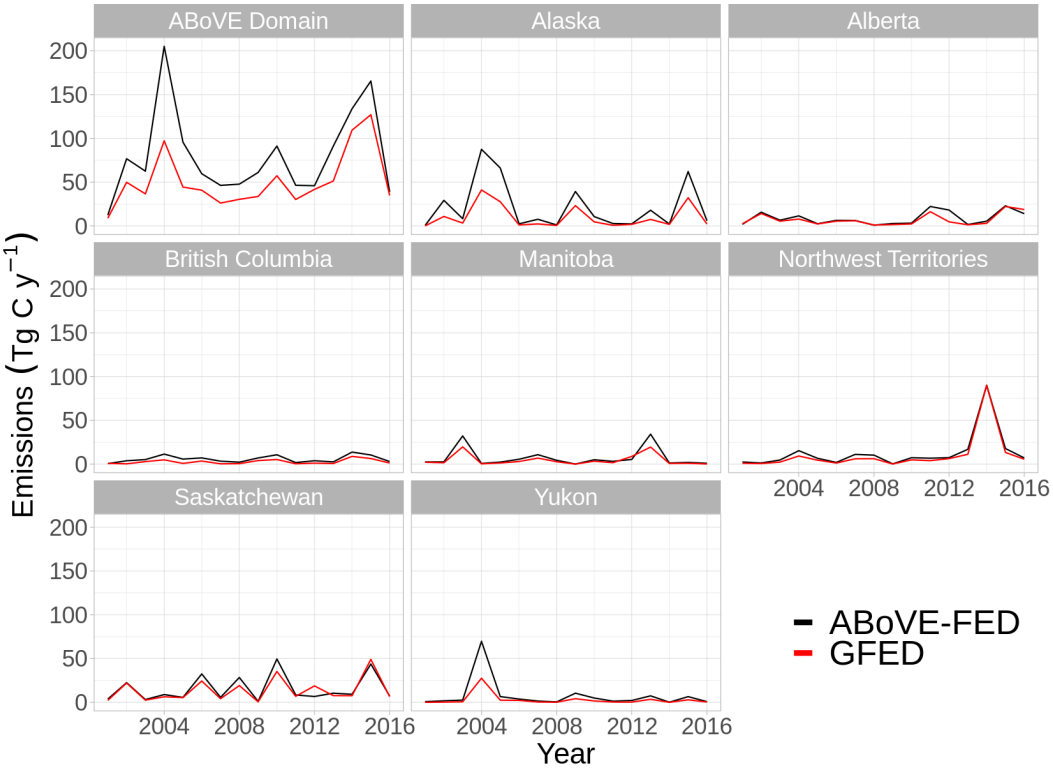

Figure S23. Total carbon emissions for ABoVE-FED and GFED in the ABoVE Domain, Alaska, and Canadian provinces and territories between 2001 -2016.

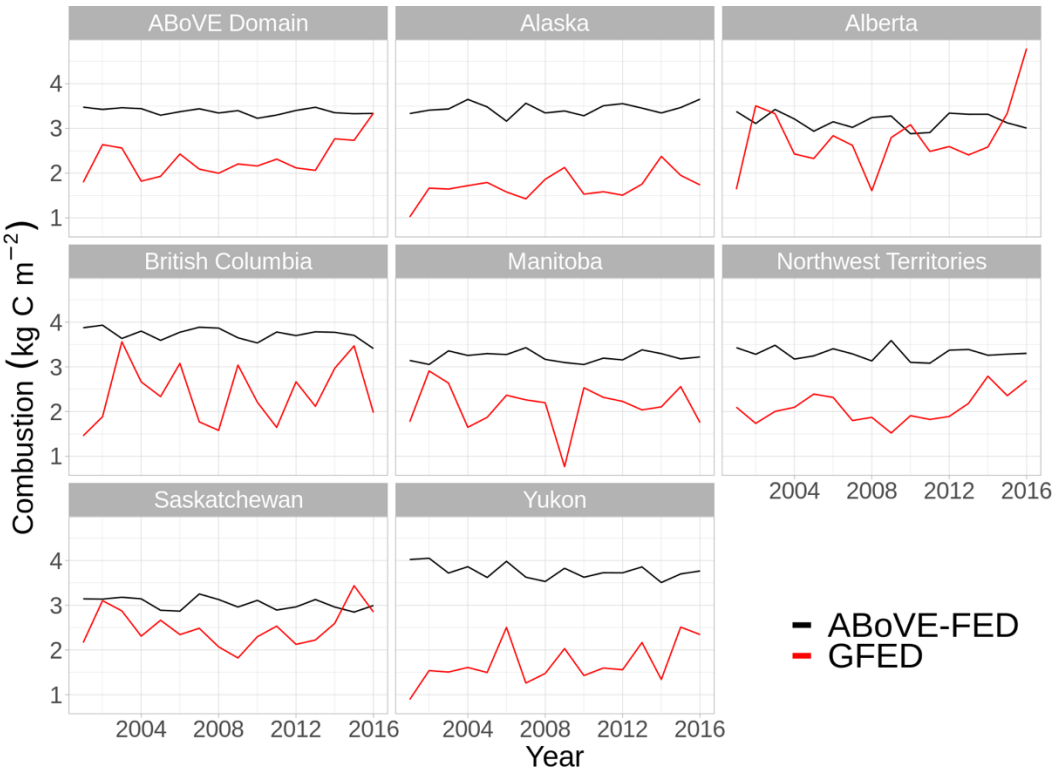

Figure S24. Mean combustion for ABoVE-FED and GFED in the ABoVE Domain, Alaska, and Canadian provinces and territories between 2001 -2016.

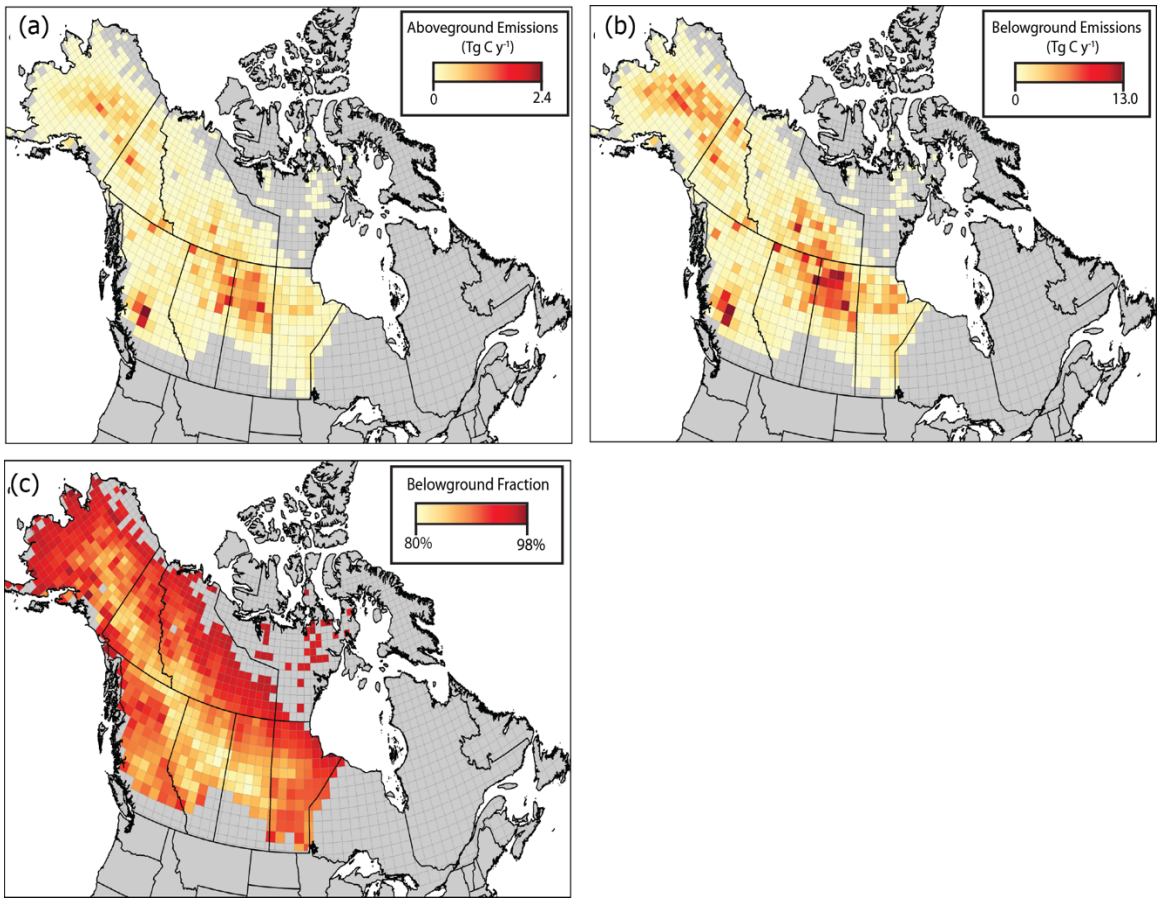

Figure S25. Aboveground carbon emissions (a), belowground carbon emissions (b), and the fraction of total emissions coming from belowground (c) from 2001-2019 aggregated to a 70 km grid.

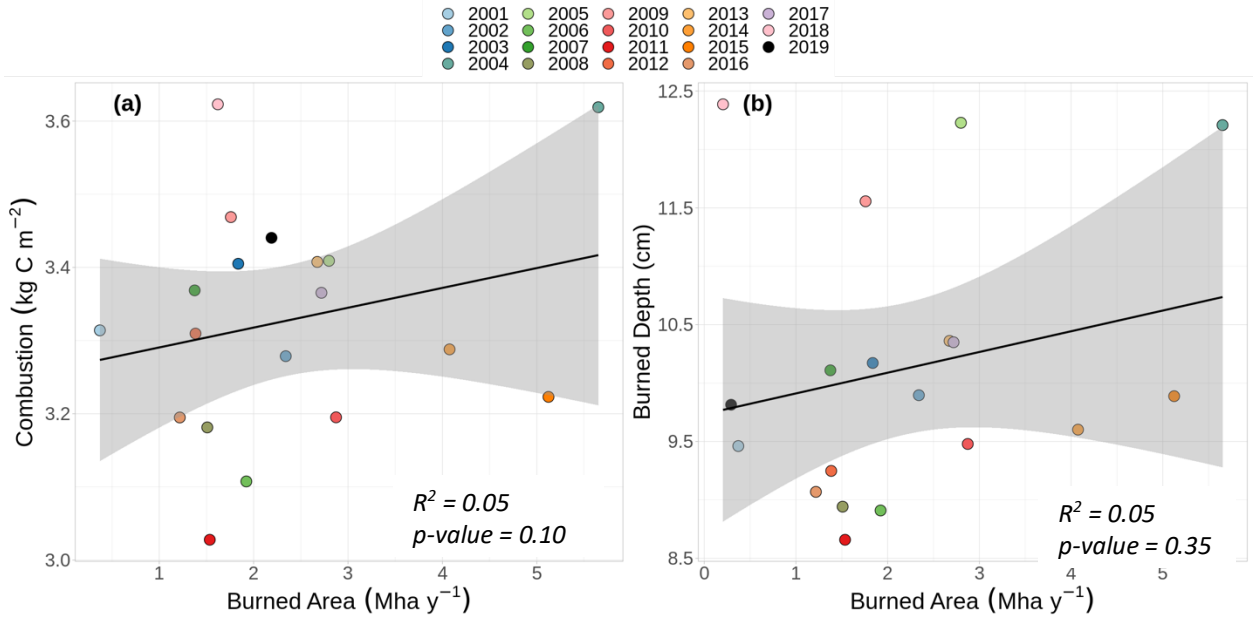

Figure S26. Mean combustion (a) and burn depth (b) as a function of annual burned area. 95% confidence intervals are shown in gray.

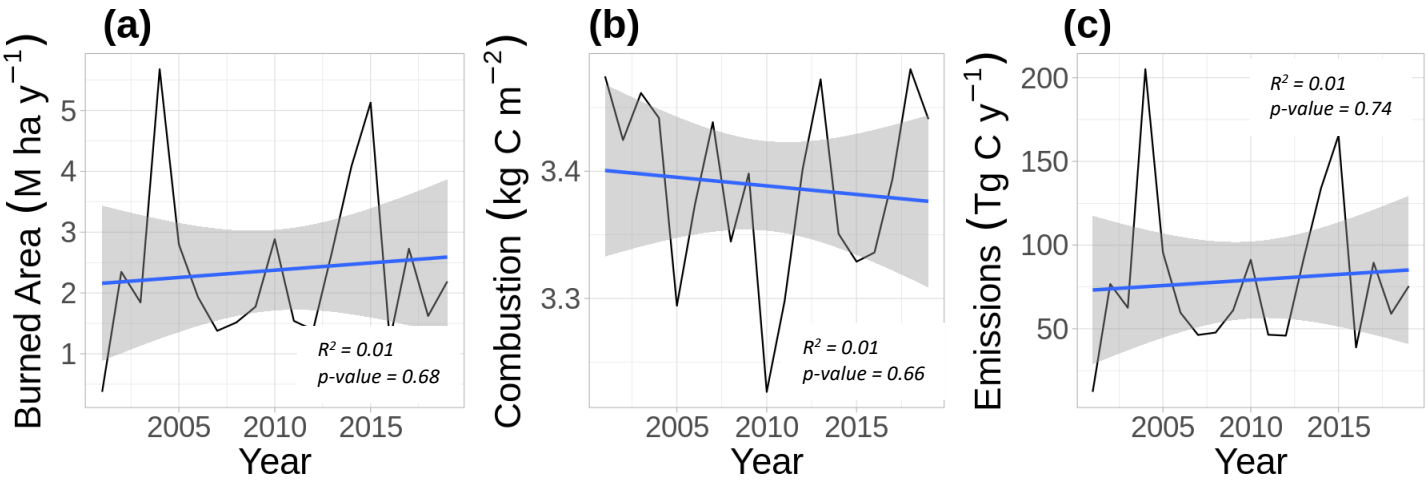

Figure S27. Trends in burned area (a), combustion (b) and emissions (c) 2001-2019. Gray shading shows the 95% confidence interval.

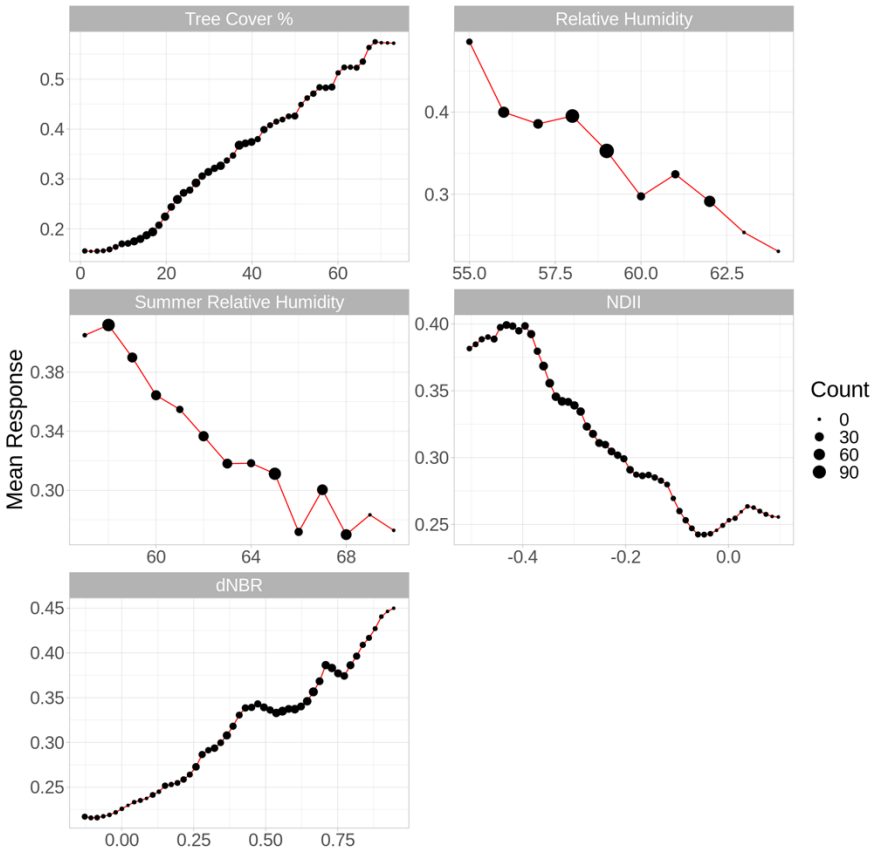

Figure S28. Partial dependence plots for the five most important variables for the primary aboveground combustion model. Counts shown as black dots indicate the number of observations used to calculate the partial dependence in each bin.

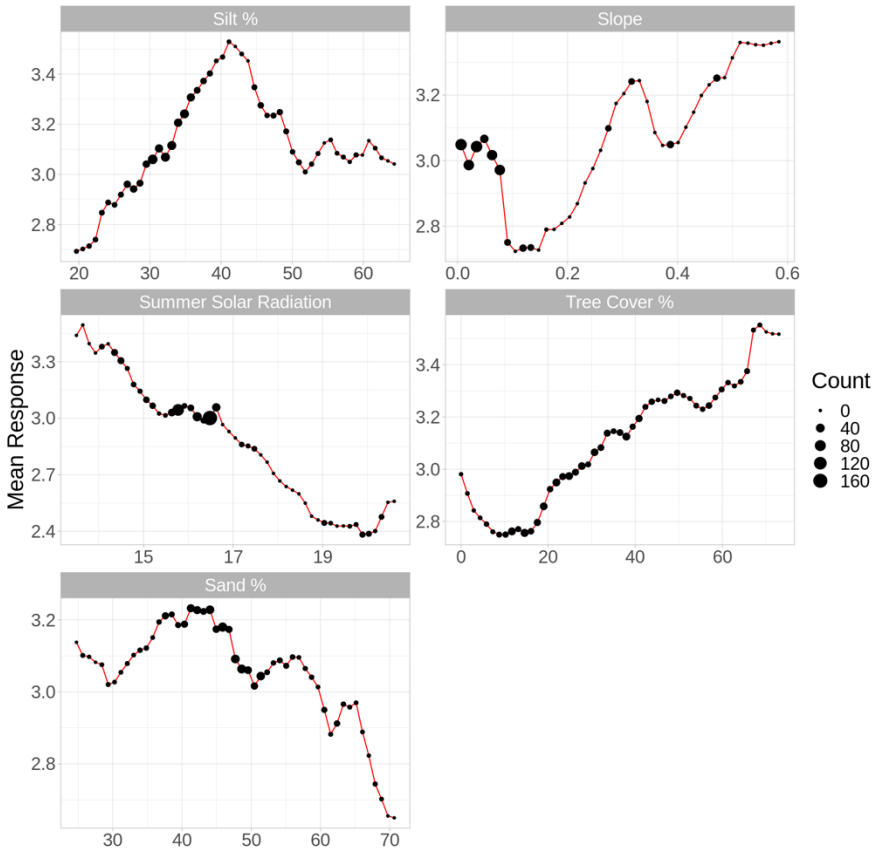

Figure S29. Partial dependence plots for the five most important variables for the primary belowground combustion model. Counts shown as black dots indicate the number of observations used to calculate the partial dependence in each bin.

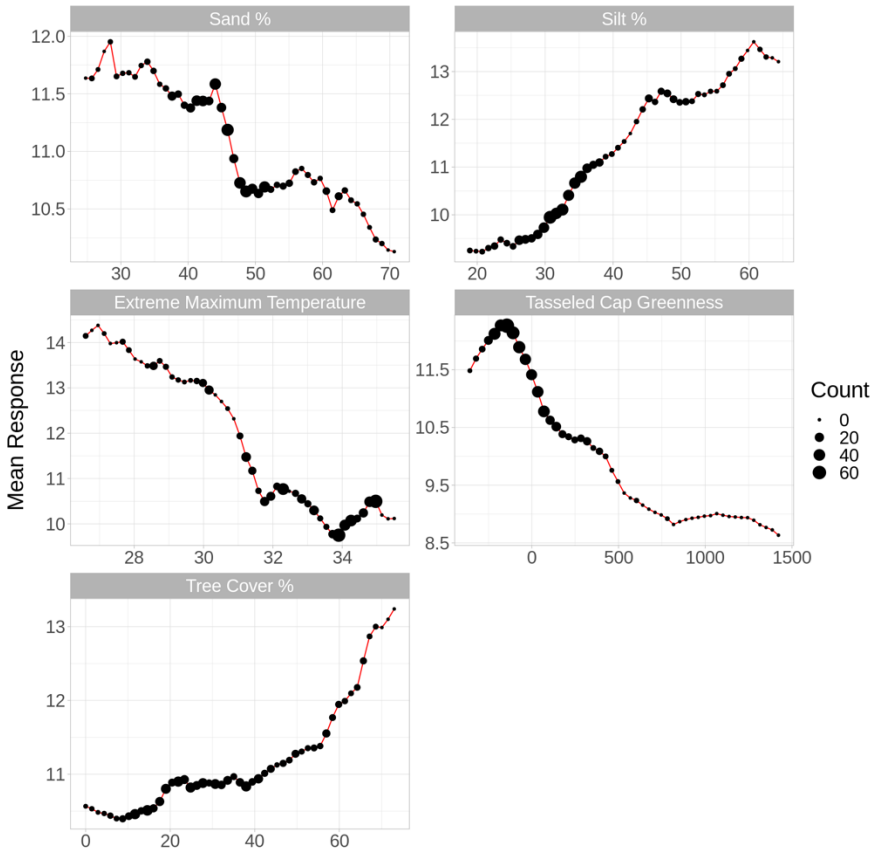

Figure S30. Partial dependence plots for the five most important variables for the primary burn depth model. Counts shown as black dots indicate the number of observations used to calculate the partial dependence in each bin.

Supplemental Tables

Table S1. Existing products compared against ABoVE-FED burned area and emissions. Columns detail their temporal availability, native resolution, spatial domain, and variable of interest as indicated by burned area (BA), carbon combustion (C) or both (BA & C). Temporal availability of the NLFD depends on states and Canadian provinces and territories, but generally begins in the mid 20th-century.

Product	Temporal Availability	Resolution	Spatial Domain	Variable of Interest
Alaska Large Fire Database and Canadian National Fire Database (NLFD)[1]	<=2001-Present	Vector based	Alaska/Canada	BA
Canadian National Burned Area Composite (NBAC)[2]	1985-Present	Vector based	Canada	BA
MCD64A1 Collection 5	2001-2015	500 m	Global	BA
MCD64A1 Collection 6[3]	2001-Present	500 m	Global	BA
Alaska Fire Emission Database version 2	2001-2015	500 m	Alaska, Yukon Territory, Northwestern Territories	BA & C
Global Fire Emission Database 4s (GFED 4s)[4]	2001-2016	0.25°x 0.25°	Global	BA & C
Fire Model Intercomparison Product (FireMIP)[5]	2001-2012	0.5° - 2.8125°	Global	BA & C

[1]Kasischke, E. S., Williams, D., & Barry, D. (2002). Analysis of the patterns of large fires in the boreal forest region of Alaska. *International Journal of Wildland Fire*, *11*(2), 131–144. https://doi.org/10.1071/wf02023

[1]Amiro, B. D., Todd, J. B., Wotton, B. M., Logan, K. A., Flannigan, M. D., Stocks, B. J., Mason, J. A., Martell, D. L., & Hirsch, K. G. (2001). Direct carbon emissions from Canadian forest

fires, 1959-1999. *Canadian Journal of Forest Research*, *31*(3), 512–525. https://doi.org/10.1139/cjfr-31-3-512

[1]Stocks, B. J., Mason, J. A., Todd, J. B., Bosch, E. M., Wotton, B. M., Amiro, B. D., Flannigan, M. D., Hirsch, K. G., Logan, K. A., Martell, D. L., & Skinner, W. R. (2003). Large forest fires in Canada, 1959–1997. *Journal of Geophysical Research: Atmospheres*, *107*(D1), FFR 5-1-FFR 5-12. https://doi.org/10.1029/2001JD000484

[2]Hall, R. J., Skakun, R. S., Metsaranta, J. M., Landry, R., Fraser, R. H., Raymond, D., Gartrell, M., Decker, V., Little, J., Hall, R. J., Skakun, R. S., Metsaranta, J. M., Landry, R., Fraser, R. H., Raymond, D., Gartrell, M., Decker, V., & Little, J. (2020). Generating annual estimates of forest fire disturbance in Canada: The National Burned Area Composite. *International Journal of Wildland Fire*, *29*(10), 878–891. https://doi.org/10.1071/WF19201

[3]Giglio, L., Boschetti, L., Roy, D. P., Humber, M. L., & Justice, C. O. (2018). The Collection 6 MODIS burned area mapping algorithm and product. *Remote Sensing of Environment*, *217*, 72–85. https://doi.org/10.1016/j.rse.2018.08.005

[4]van der Werf, G. R., Randerson, J. T., Giglio, L., van Leeuwen, T. T., Chen, Y., Rogers, B. M., Mu, M., van Marle, M. J. E., Morton, D. C., Collatz, G. J., Yokelson, R. J., & Kasibhatla, P. S. (2017). Global fire emissions estimates during 1997–2016. *Earth System Science Data*, *9*(2), 697–720. https://doi.org/10.5194/essd-9-697-2017

[5]Rabin, S. S., Melton, J. R., Lasslop, G., Bachelet, D., Forrest, M., Hantson, S., Kaplan, J. O., Li, F., Mangeon, S., Ward, D. S., Yue, C., Arora, V. K., Hickler, T., Kloster, S., Knorr, W., Nieradzik, L., Spessa, A., Folberth, G. A., Sheehan, T., … Arneth, A. (2017). The Fire Modeling Intercomparison Project (FireMIP), phase 1: Experimental and analytical protocols with detailed model descriptions. *Geoscientific Model Development*, *10*(3), 1175–1197. https://doi.org/10.5194/gmd-10-1175-2017

[5]Hantson, S., Arneth, A., Harrison, S. P., Kelley, D. I., Prentice, I. C., Rabin, S. S., Archibald, S., Mouillot, F., Arnold, S. R., Artaxo, P., Bachelet, D., Ciais, P., Forrest, M., Friedlingstein, P., Hickler, T., Kaplan, J. O., Kloster, S., Knorr, W., Lasslop, G., … Yue, C. (2016). The status and challenge of global fire modelling. *Biogeosciences*, *13*(11), 3359–3375. https://doi.org/10.5194/bg-13-3359-2016

Table S2. Variables initially evaluated for combustion and burn depth models. Any climate variable listing "Summer" represents the 1981-2010 June – August means, and all other variables represent annual means. If a variable does not list "Spring" (March-May) or "Summer" (June-August), it represents an annual mean for the year of fire. Variables marked with "^" indicate they were retained for the primary aboveground combustion model, "*" indicates they were retained for the primary belowground combustion model, and '&' indicates they were retained for the primary burn depth model.

Variable	**Unit**	**Source**
Clay	%	SoilGrids[1]*&
Sand	%	SoilGrids*&
Silt	%	SoilGrids^*&
Bulk density	g cm^{-3}	SoilGrids^*&
Soil organic carbon stock	tons ha^{-1}	SoilGrids^*&
Soil water pH	pH	SoilGrids*&
Elevation	Meters	Burns[2]^*&
Aspect	Degrees	Burns
Slope	Degrees	Burns*
Topographic wetness index	Unitless	Burns
Permafrost zonation index	0-1	Gruber[3]*&
Surface ruggedness index	0-1	Gruber*&
Mean annual temperature	°C	ClimateNA[4]
Mean summer temperature	°C	ClimateNA
Mean maximum annual temperature	°C	ClimateNA*&
Mean summer maximum temperature	°C	ClimateNA
Mean minimum annual temperature	°C	ClimateNA*&
Mean summer minimum temperature	°C	ClimateNA*&
Mean annual precipitation	mm/y	ClimateNA&
Mean summer precipitation	mm/y	ClimateNA*
Mean annual degree days > 18°C	Days	ClimateNA&
Mean summer degree days > 18°C	Days	ClimateNA*
Mean annual degree days < 18°C	Days	ClimateNA*
Mean summer degree days < 18°C	Days	ClimateNA*&
Mean annual Degree days > 5°C	Days	ClimateNA^*
Mean summer Degree days > 5°C	Days	ClimateNA$
Mean annual Degree days < 0°C	Days	ClimateNA^*&
Mean annual precipitation as snow	Mm/y	ClimateNA*&
Mean summer precipitation as snow	Mm/y	ClimateNA
Mean annual frost free period	# of Days	ClimateNA
Beginning frost free period	Julian Day	ClimateNA
Ending frost free period	Julian Day	ClimateNA
Mean annual heat moisture index	Unitless	ClimateNA*
Mean summer heat moisture index	Unitless	ClimateNA
Mean annual reference evapotranspiration	mm/y	ClimateNA*
Mean summer reference evapotranspiration	mm/y	ClimateNA&
Mean annual climatic moisture deficit	Mm/y	ClimateNA&

Mean summer climatic moisture deficit	mm	ClimateNA*
Mean annual relative humidity	Unitless	ClimateNA^&
Mean summer relative humidity	Unitless	ClimateNA^
Mean annual solar radiation	MJ m^{-2} d^{-}	ClimateNA*
Mean summer solar radiation	MJ m^{-2} d^{-}	ClimateNA*
Mean annual warmest month temperature	°C	ClimateNA
Mean annual coldest month temperature	°C	ClimateNA
Temperature Differential of warmest and coldest month	°C	ClimateNA&
Extreme maximum temperature 1981 - 2010	°C	ClimateNA*&
Extreme minimum temperature 1981 - 2010	°C	ClimateNA^*&
Buildup Index	Unitless	GFWED[5]^&
Drought Code	Unitless	GFWED*
Duff Moisture Code	Unitless	GFWED&
Daily Severity Rating	Unitless	GFWED
Initial Spread Index	Unitless	GFWED
Fine Fuel Moisture Code	Unitless	GFWED
Fire Weather Index	Unitless	GFWED
Vapor Pressure Deficit	mm	GFWED
Wind Speed	km/hour	GFWED*
Relative Humidity	Unitless	GFWED*&
Temperature	°C	GFWED
NDVI	Unitless	Landsat/MODIS[6]*&
NDII	Unitless	Landsat/MODIS[7]^*&
dNBR	Unitless	Landsat/MODIS[8]^*&
RdNBR	Unitless	Landsat/MODIS[9]^*&
RBR	Unitless	Landsat/MODIS[10]^*&
Tasselled Cap Greeness	Unitless	Landsat/MODIS[11]*&
Tasselled Cap Wetness	Unitless	Landsat/MODIS[11]*&
Tasselled Cap Brightness	Unitless	Landsat/MODIS[11]^*&
Tree cover	Percent	Sexton[12]^*&
Day of Burn	Julian Day	Walker et al. 2020[13] *&
Jack Pine	Percent	Beaudoin & Ottmar[14]*
White Spruce	Percent	Beaudoin & Ottmar[14]*&
Black Spruce	Percent	Beaudoin & Ottmar[14]*&
Deciduous	Percent	Beaudoin & Ottmar[14]*&
Grass/Shrub	Percent	Beaudoin & Ottmar[14]
Other Conifers	Percent	Beaudoin & Ottmar[14]
Non Vegetated	Percent	Beaudoin & Ottmar[14]*&

[1]Hengl, T., Mendes De Jesus, J., Heuvelink, G. B. M., Gonzalez, M. R., Kilibarda, M., Blagotić, A., … Blagotić, M. (2017). SoilGrids250m: Global gridded soil information based on machine learning. *PLOS ONE*, *12*(2), 1–40. https://doi.org/10.1371/journal

[2] Burns, PJ, Massey, RM, Shean, D, Husby, EB, Goetz, SG, (2022). A composite 10-m digital elevation model of Alaska and Canada for NASA ABoVE. In preparation for Environmental Research Letters

[3] Gruber, S. (2012). Derivation and analysis of a high-resolution estimate of global permafrost zonation. *The Cryosphere*, *6*, 221–233. https://doi.org/10.5194/tc-6-221-2012

[4] Wang, T., Hamann, A., Spittlehouse, D., & Carroll, C. (2016b). Locally Downscaled and Spatially Customizable Climate Data for Historical and Future Periods for North America. *PLOS ONE*. https://doi.org/10.1371/journal.pone.0156720

[5]Field, R.D., A.C. Spessa, N.A. Aziz, A. Camia, A. Cantin, R. Carr, W.J. de Groot, A.J. Dowdy, M.D. Flannigan, K. Manomaiphiboon, F. Pappenberger, V. Tanpipat, and X. Wang, 2015: Development of a global fire weather database. *Nat. Hazards Earth Syst. Sci.*, **15**, 1407-1423, doi:10.5194/nhess-15-1407-2015.

[6]Tucker, C. J. (1979). Red and photographic infrared linear combinations for monitoring vegetation. Remote Sensing of Environment, 8, 127–150.

[7]Hardisky, M. A., Klemas, V., & Smart, R. M. (1983). The influences of soil salinity, growth form, and leaf moisture on the spectral reflectance of Spartina alterniflora canopies. Photogrammetric Engineering and Remote Sensing, 49, 77–83.

[8]Key, C.H.; Benson, N.C. Landscape assessment (LA). In FIREMON: Fire Effects Monitoring and Inventory System; General Technical Report RMRS-GTR-164-CD; U.S. Department of Agriculture, Forest Service, Rocky Mountain Research Station: Fort Collins, CO, USA, 2006.

[9]Miller, J.D.; Thode, A.E. Quantifying burn severity in a heterogeneous landscape with a relative version of the delta Normalized Burn Ratio (dNBR). Remote Sens. Environ. 2007, 109, 66–80.

[10]Holden, Z.A.; Morgan, P.; Evans, J.S. A predictive model of burn severity based on 20-year satellite-inferred burn severity data in a large southwestern US wilderness area. For. Ecol. Manag. 2009, 258, 2399–2406.

[11]Kauth, R.J. and Thomas, G.S. 1976, The Tasselled Cap—A Graphic Description of the Spectral–Temporal Development of Agricultural Crops as Seen by LANDSAT. LARS Symposia, paper 159.

[12]Sexton, J. O., Song, X.-P., Feng, M., Noojipady, P., Anand, A., Huang, C., Kim, D.-H., Collins, K.M., Channan, S., DiMiceli, C., Townshend, J.R.G. (2013). Global, 30-m resolution continuous fields of tree cover: Landsat-based rescaling of MODIS Vegetation Continuous Fields with lidar-based estimates of error. International Journal of Digital Earth, 130321031236007. doi:10.1080/17538947.2013.786146.

[13] Walker, X.J., J.L. Baltzer, L.L. Bourgeau-Chavez, N.J. Day, W.J. De groot, C. Dieleman, E.E. Hoy, J.F. Johnstone, E.S. Kane, M.A. Parisien, S. Potter, B.M. Rogers, M.R. Turetsky, S. Veraverbeke, E. Whitman, and M.C. Mack. 2019. ABoVE: Synthesis of Burned and Unburned Forest Site Data, AK and Canada, 1983-2016. ORNL DAAC, Oak Ridge, Tennessee, USA. https://doi.org/10.3334/ORNLDAAC/1744

[14]Beaudoin, A., P. Y. Bernier, L. Guindon, P. Villemaire, X. J. Guo, G. Stinson, T. Bergeron, S. Magnussen, and R. J. Hall (2014), Mapping attributes of Canada's forests at moderate resolution through kNN and MODIS imagery, *Can. J. For. Res.*, *44*(5), 521–532, doi:10.1139/cjfr-2013-0401.

[14]Ottmar, R. D., D. V. Sandberg, C. L. Riccardi, and S. J. Prichard (2007), An overview of the Fuel Characteristic Classification System - Quantifying, classifying, and creating fuelbeds for resource planning, *Can. J. For. Res.*, *37*(12), 2383–2393, doi:10.1139/X07-077.

[15]Walker, X.J., J.L. Baltzer, L.L. Bourgeau-Chavez, N.J. Day, W.J. De groot, C. Dieleman, E.E. Hoy, J.F. Johnstone, E.S. Kane, M.A. Parisien, S. Potter, B.M. Rogers, M.R. Turetsky, S. Veraverbeke, E. Whitman, and M.C. Mack. 2020a. ABoVE: Synthesis of Burned and Unburned Forest Site Data, AK and Canada, 1983-2016. ORNL DAAC, Oak Ridge, Tennessee, USA. https://doi.org/10.3334/ORNLDAAC/1744

Table S3. Final model parameters selected for the primary ranger random forest model.

Model	Number of variables sampled at each split	Split Rule	Minimum Node Size
Aboveground Combustion	10	extraTrees	5
Belowground Combustion	7	extraTrees	5
Burn Depth	9	extraTrees	7

Table S4. Comparison of ABoVE-FED total carbon emissions and mean per-pixel combustion against AKFED fires in 2004, Walker et al., 2018 for the 2014 Northwest Territories (NWT) fires, Deielemen et al., 2020 for the 2015 Saskatchewan (SK) fires, and GFED4s for 2001-2016 fires in the ABoVE-extended domain. Uncertainty in emissions and mean combustion are shown when available.

Domain, year	Source	Total Emissions (Tg C y^{-1})	Mean combustion (kg C m^{-2})
Northwest Territories, 2014	ABoVE-FED	89.7 (±38.60)	2.89 (±1.16)
	Walker et al. (2018)	94.3 (± 7.9)	3.31 (±0.30)
	AKFED	164 (± 32)	4.81
Saskatchewan, 2015	ABoVE-FED	39.17 (±18.47)	2.43 (±1.21)
	Dieleman et al. (2020)	36.3 (± 15.0)	2.5 (1.10)
Alaska, 2001-2015	ABoVE-FED	22.2 (±10.14)	3.34 (±1.46)
	AKFED	18.9	3.03
Northwest Territories, 2001-2015	ABoVE-FED	12.2 (±5.15)	3.29 (±1.11)
	AKFED	18.8	3.44
Yukon Territory, 2001-2015	ABoVE-FED	7.49 (± 4.00)	3.71 (±1.90)
	AKFED	5.00	2.26
ABoVE extended domain, 2001-2016	ABoVE-FED	80 (±21.67)	3.39 (±1.17)
	GFED	51	2.30

Table S5. Multiple regression results in Alaska and the ABoVE Extended Domain when regressing depth of burn and belowground combustion against annual burned area and Julian day of burn (DOB). * Indicates significant slopes at p-value <= 0.05 and ** indicates significant slopes at p-values <= 0.01. Multiple regression models were implemented using both the field dataset used in model training and a sample of 500 pixels between 2001-2019 from ABoVE-FED.

Area of Interest	**Database**	**Independent Variable**	**Burned Area slope**	**DOB slope**
Alaska	Field	Burn Depth	0.431	0.0006
	ABoVE-FED	Belowground Combustion	0.126**	0.0010
ABoVE Extended Domain	Field	Burn Depth	1.11**	-0.013**
	ABoVE-FED	Belowground Combustion	0.0223	0.00162*

Table S6. Influence of Julian day of burn (DOB) on burn depth and belowground combustion in years of differing burned area, represented by quantiles. Quantile 1 contains the smallest fire years, and quantile 4 the largest. * Indicates significant slopes at p-value <= 0.05 and ** indicates significant slopes at p-values <= 0.01. Multiple regression models were implemented using both the field dataset used in model training and a sample of 500 pixebetween 2001-2019 from ABoVE-FED.

Area of Interest	**Database**	**Independent Variable**	**Quantile**	**DOB slope**
Alaska	Field	Burn Depth	1	-0.0324
			2	0.0699*
			3	0.0181
			4	-0.0399
	ABoVE-FED	Burn Depth	1	-0.0047*
			2	-0.0081*
			3	0.0116**
			4	0.0052
	Field	Belowground Combustion	1	0.0037**
			2	0.0014**
			3	0.0019**
			4	0.0003**
	ABoVE-FED	Belowground Combustion	1	0.0582**
			2	0.0240
			3	0.0018**
			4	-0.0002
ABoVE Extended Domain	Field	Burn Depth	1	-0.0012
			2	-0.0131
			3	-0.0281
			4	0.0278
	ABoVE-FED	Burn Depth	1	0.0155**
			2	0.0042**
			3	0.0077**
			4	0.0052**
	Field	Belowground Combustion	1	0.0054**
			2	0.0029**
			3	0.0021**
			4	0.0036**
	ABoVE-FED	Belowground Combustion	1	0.0155**
			2	0.0042**
			3	0.0079**
			4	0.0052**

References

Breiman, L.: Random Forests. Machine Learning, 45(1), 5–32. https://doi.org/10.1023/A:1010933404324, 2001.

Cortes, C., and Vapnik, V.: Support-vector networks. Machine Learning, 20(3), 273–297. https://doi.org/10.1007/BF00994018, 1995.

Hoerl, A. E., and Kennard, R. W.: Ridge Regression: Biased Estimation for Nonorthogonal Problems. Technometrics, 12(1), 55–67. https://doi.org/10.1080/00401706.1970.10488634, 1970.

Karatzoglou, A., Smola, A., Hornik, K., Zeileis, A.: kernlab - An S4 Package for Kernel Methods in R. Journal of Statistical Software 11(9), 1-20. URL http://www.jstatsoft.org/v11/i09/, 2004.

Meinshausen, N.: quantregForest: Quantile Regression Forests. R package version 1.3-7. https://CRAN.R-project.org/package=quantregForest, 2017.

Meyer, D., Dimitriadou, E., Hornik, K., Weingessel, A., and Leisch, F.: e1071: Misc Functions of the Department of Statistics, Probability Theory Group (Formerly: E1071), TU Wien. Package version 1.7-9. https://CRAN.R-project.org/package=e1071, 2021.

R Core Team.: R: A language and environment for statistical computing. R Foundation for Statistical Computing, Vienna, Austria. URL https://www.R-project.org/, 2021.

Tibshirani, R. Regression Shrinkage and Selection Via the Lasso. Journal of the Royal Statistical Society: Series B (Methodological), 58(1), 267–288. https://doi.org/10.1111/j.2517-6161.1996.tb02080.x, 1996.

Wright, M., and Ziegler, A.: ranger: A Fast Implementation of Random Forests for High Dimensional Data in C++ and R. Journal of Statistical Software, 77(1), 1-17. doi:10.18637/jss.v077.i01, 2017.

Zou H., and Hastie, T..: elasticnet: Elastic-Net for Sparse Estimation and Sparse PCA. R package version 1.3. https://CRAN.R-project.org/package=elasticnet, 2020.